AGU PUBLICATIONS

Journal of Advances in Modeling Earth Systems

RESEARCH ARTICLE

10.1002/2016MS000826

Satellite radiance data assimilation for binary tropical cyclone cases over the western North Pacific

Yonghan Choi[1,2], Dong-Hyun Cha[1], Myong-In Lee[1], Joowan Kim[3], Chun-Sil Jin[1,4], Sang-Hun Park[5], and Min-Su Joh[6]

[1]School of Urban and Environmental Engineering, Ulsan National Institute of Science and Technology, Ulsan, Korea, [2]National Center for Atmospheric Research, Boulder, Colorado, USA, [3]Department of Atmospheric Sciences, Kongju National University, Gongju, Korea, [4]Environmental Modeling Center, NOAA/NWS/NCEP, College Park, Maryland, USA, [5]Department of Atmospheric Sciences, Yonsei University, Seoul, Korea, [6]Korea Institute of Science and Technology Information, Daejeon, Korea

Key Points:
- Satellite radiance data assimilation is effective in improving track forecasts of binary tropical cyclones
- Improved forecasts of environmental fields result in reduced track errors for binary tropical cyclones
- Positive effects of satellite radiance data assimilation can be limited when a direct interaction between binary tropical cyclones exists

Correspondence to:
D.-H. Cha,
dhcha@unist.ac.kr

Citation:
Choi, Y., D.-H. Cha, M.-I. Lee, J. Kim, C.-S. Jin, S.-H. Park, and M.-S. Joh (2017), Satellite radiance data assimilation for binary tropical cyclone cases over the western North Pacific, *J. Adv. Model. Earth Syst.*, *9*, 832–853, doi:10.1002/2016MS000826.

Received 5 OCT 2016
Accepted 15 MAR 2017
Accepted article online 17 MAR 2017
Published online 13 APR 2017

Abstract A total of three binary tropical cyclone (TC) cases over the Western North Pacific are selected to investigate the effects of satellite radiance data assimilation on analyses and forecasts of binary TCs. Two parallel cycling experiments with a 6 h interval are performed for each binary TC case, and the difference between the two experiments is whether satellite radiance observations are assimilated. Satellite radiance observations are assimilated using the Weather Research and Forecasting Data Assimilation (WRFDA)'s three-dimensional variational (3D-Var) system, which includes the observation operator, quality control procedures, and bias correction algorithm for radiance observations. On average, radiance assimilation results in slight improvements of environmental fields and track forecasts of binary TC cases, but the detailed effects vary with the case. When there is no direct interaction between binary TCs, radiance assimilation leads to better depictions of environmental fields, and finally it results in improved track forecasts. However, positive effects of radiance assimilation on track forecasts can be reduced when there exists a direct interaction between binary TCs and intensities/structures of binary TCs are not represented well. An initialization method (e.g., dynamic initialization) combined with radiance assimilation and/or more advanced DA techniques (e.g., hybrid method) can be considered to overcome these limitations.

1. Introduction

Tropical cyclone (TC) forecasts have improved in the past two decades. Errors in TC track forecasts are significantly reduced, and TC intensity forecasts also show notable improvements [*Rappaport et al*., 2009]. This substantial progress can be attributed to advances in numerical weather prediction (NWP) models (e.g., numerical and physics schemes), data assimilation (DA) and initialization methods (e.g., hybrid DA and dynamic initialization methods), and observing platforms (e.g., satellite and radar observations). However, despite these advancements, numerical forecast of TCs is still a challenging issue due to complex nature of TC development. Particularly, when two or more TCs exist simultaneously in the same region, predictability of the track and intensity of an individual TC can be further limited because of the interaction between TCs [*Jarrell et al*., 1978].

Since the pioneering work of *Fujiwhara* [1921, 1923], there have been a number of observational and modeling studies on the interaction between binary TCs. Observational studies have investigated the characteristics of binary TCs in the western North Pacific (WNP) using best track data [*Brand*, 1970; *Dong and Neumann*, 1983; *Lander and Holland*, 1993; *Carr et al*., 1997; *Wu et al*., 2011; *Jang and Chun*, 2015a], satellite imagery [*Kuo et al*., 2000], and reanalysis [*Wu et al*., 2003]. Among these studies, *Lander and Holland* [1993] found that the classical Fujiwhara model was rarely observed, and instead, they suggested a modified model of binary interaction that included approach, capture, cyclonic orbit, and merger/escape. *Carr et al*. [1997] proposed four conceptual models for binary interaction: direct, semidirect, indirect interactions, and reverse-oriented monsoon trough formation (refer to *Carr et al*. [1997] for details).

Previous studies with nondivergent barotropic models primarily focused on the critical separation distance for mutual interaction, attraction, or repulsion, and the factors that determined the degree of binary

interaction [*Chang*, 1983; *DeMaria and Chan*, 1984; *Ritchie and Holland*, 1993; *Prieto et al*., 2003]. The interaction between binary TCs is more complicated, and it is significantly affected by baroclinicity in a three-dimensional framework [*Wang and Holland*, 1995; *Khain et al*., 2000; *Wu et al*., 2012; *Jang and Chun*, 2015b]. *Wang and Holland* [1995] utilized a three-dimensional primitive-equation model to investigate the binary interaction of TCs, and they found two critical separation distances: mutual approach separation (MAS) and mutual merger separation (MMS).

Along with improved numerical models, assimilation of satellite data has improved predictability of TCs by reducing uncertainties in initial conditions. Conventional observations from radiosondes, aircrafts, profilers, and land/oceanic surface stations can provide useful information on the atmosphere, but their spatial/temporal coverage and resolution are limited. Satellite radiance data are particularly useful because they provide information over the ocean, where conventional observations are sparse, and TCs are mainly located. Satellite radiance data are currently assimilated at most operational NWP centers, and they are one of the most important observation types for global NWP, especially over the regions where the number of in situ observations is small [*Derber and Wu*, 1998; *McNally et al*., 2000; *Zapotocny et al*., 2008; *Zhu and Gelaro*, 2008; *Cardinali*, 2009; *Joo et al*., 2013]. DA methods for assimilation of radiance observations in the global NWP have been changed from variational methods or ensemble-based methods to hybrid (hybrid of variational and ensemble-based methods) methods [*Bonavita et al*., 2015; *Lorenc et al*., 2015]. Radiance observations affected by cloud or precipitation have potentially more useful information than clear-sky radiance observations. Currently, at most NWP centers, various forms of all-sky radiance observations are assimilated [*Bauer et al*., 2011; *Kazumori et al*., 2016; *Zhu et al*., 2016], but all-sky radiance assimilation has some limitations because of its complexity.

There have been a number of studies on satellite data assimilation for regional TC forecasts using variational [*Chen et al*., 2004; *Singh et al*., 2011, 2012; *Xu et al*., 2013; *Zou et al*., 2013a,b], ensemble-based [*Liu et al*., 2012; *Schwartz et al*., 2012; *Newman et al*., 2015], and hybrid [*Xu et al*., 2015] DA methods. *Schwartz et al*. [2012] conducted data assimilation experiments with a cyclic, limited-area ensemble adjustment Kalman filter (EAKF) for a 1 week period to evaluate the effects of assimilating microwave radiances on track, intensity, and precipitation forecasts of Typhoon Morakot (2009). They suggested that assimilating microwave radiances with a limited-area EAKF was beneficial for TC forecasts, but the degree of improvement differed among track, intensity, and precipitation forecasts.

Following *Schwartz et al*. [2012], *Liu et al*. [2012] investigated the impact of assimilating Advanced Microwave Sounding Unit-A (AMSU-A) radiances on the forecasts of several TCs over the Atlantic Ocean for a monthlong period using a limited-area ensemble Kalman filter (EnKF). They found that assimilating AMSU-A radiances produced better depiction of the environmental fields and resulted in substantial improvement of TC track and intensity forecasts. The impact of assimilating Infrared Atmospheric Sounding Interferometer (IASI) radiances on the analyses and forecasts of Hurricane Maria (2011) and Typhoon Megi (2010) was examined using the three-dimensional variational (3D-Var) method in *Xu et al*. [2013]. They implemented the cloud-detection scheme of *McNally and Watts* [2003] into the Weather Research and Forecasting Data Assimilation (WRFDA) system to exclude cloud-contaminated IASI radiances when assimilating radiance observations. Assimilation of IASI radiances had a consistent positive impact on the forecast skills for track, minimum sea level pressure, and maximum wind speed of TCs.

Although satellite radiance data assimilation has shown its potential for improving TC forecasts both in global and regional model applications, it is expected that more careful considerations should be given for binary TC forecasts due to complexities in binary TCs' interaction. *Jang and Chun* [2015a] indicated that the poleward steering flow, weaker vertical wind shear, and warmer sea surface temperatures are favorable conditions for occurring binary TCs because these factors result in a longer lifetime of TCs, which can increase the probability that multiple TCs exist simultaneously. Recently, warmer sea surface temperatures are frequently observed due to global warming [*Saba et al*., 2016; *Wijffels et al*., 2016], and this can provide favorable conditions for binary TCs. For example, in 2015, binary TCs (Chan-hom/Nangka) were developed over the WNP in July, and even three category-4 hurricanes (Kilo, Ignacio, and Jimena) were observed simultaneously over the Pacific Ocean in August. Operational forecasts of binary TCs (e.g., Bolaven/Tembin (2012) and Chan-hom/Nangka (2015)) from different operational centers often diverge because of low predictability of binary TCs and limited understanding about them. Therefore, research on predictability of binary TCs is needed, but there are few previous studies on this.

The objective of this study is to investigate the impacts and limits of satellite radiance data assimilation for binary TC forecasts. This is very useful and practical information for operational forecasts of TCs, but it is rarely documented in previous literature. In this study, cycling experiments are conducted for selected binary TC cases, and the effects of radiance assimilation on track and intensity forecasts of binary TCs are examined. To the best of authors' knowledge, this study is the first attempt to examine the impact of satellite radiance data assimilation on binary TC forecasts and the dynamical/physical implications underneath the results. A brief description of each binary TC case is presented in section 2, followed by model configuration and experimental design in section 3. Results and the corresponding discussions are given in section 4, and finally, section 5 includes summary and conclusions.

2. Binary Tropical Cyclone Cases

In this study, we selected binary tropical cyclone cases that affected the Korean Peninsula directly or indirectly for the period of 2010–2015. A total of three binary TC cases were selected: Bolaven/Tembin, Chan-hom/Nangka, and Goni/Atsani.

Figure 1 shows the best track, minimum sea level pressure (SLP), and distance between two binary TCs for each case. Best track data provided by the Regional Specialized Meteorological Center (RSMC) Tokyo typhoon center are used. Before 24 August 2012, TC Tembin moved westward within the monsoon gyre circulation. TC Bolaven moved northwestward due to the steering flow related to the western North Pacific subtropical high (WNPSH). At 00 UTC 24 August 2012, the distance between Bolaven and Tembin was about 1400 km, and it continuously decreased until 12 UTC 27. During that period, direct interaction between Bolaven and Tembin occurred. Tembin rotated cyclonically because it was relatively weak compared with Bolaven. Although Bolaven did not show rotational motion, its track was slightly deflected westward because of the direct interaction. The tracks of Bolaven and Tembin were similar to those of Nina and Ora, one of the examples of direct-interaction binary TCs in *Lander and Holland* [1993]. After the direct interaction, a reversed-oriented monsoon trough, one of the conceptual models suggested by *Carr et al*. [1997], formed, and both Bolaven and Tembin moved northeastward under the influence of a northeastward steering flow.

In contrast to the Bolaven/Tembin case, the distance between Chan-hom and Nangka was approximately 1900 km between 00 UTC 8 and 12 UTC 9 July 2015, and it increased to more than 2400 km at 18 UTC 12 July 2015. Therefore, there was no direct interaction between TCs Chan-hom and Nangka. In this case, there existed a third TC, Linfa, and it rotated cyclonically between 8 and 10 July 2015 because of the one-way influence by TC Chan-hom. Because Chan-hom was relatively larger and more intense, Chan-hom's track was not altered by Linfa. Between 8 and 11 July 2015, Chan-hom moved northwestward under the influence of a steering flow related to the WNPSH. Nangka also moved northwestward from 8 to 10 July, and it moved nearly westward after 10 July 2015. During this period, Nangka's track was mainly determined by the environmental flow. After 11 July 2015, Chan-hom turned northeastward, and its moving speed increased as a result of its weakening. From 11 to 12 July, Nangka continued to move westward, and it headed northward after 12 July 2015. The synoptic pattern composed of two TCs and WNPSH during this period was similar to one of the conceptual models suggested by *Carr et al*. [1997], the indirect interaction model.

The distance between TCs Goni and Atsani decreased from 2500 to 2100 km between 00 UTC 21 and 12 UTC 24 August 2015. However, even at 12 UTC 24 August 2015, Goni was too far away from Atsani, and hence there was no direct interaction between Goni and Atsani. Tracks of both Goni and Atsani were mainly affected by midlevel trough and ridge patterns related to the WNPSH. In detail, from 21 to 23 August 2015, Goni moved nearly northward, and afterward it moved northeastward until 20 UTC 24 August 2015. Goni headed northward again for about 6 h, and then it moved northeastward until it transitioned to an extratropical cyclone. Atsani moved northwestward from 21 to 22 August 2015, and then it turned northeastward. It continuously moved northeastward, and its moving speed increased as a result of its weakening after 12 UTC 24 August 2015.

In summary, direct interaction between binary TCs was observed only in the Bolaven/Tembin case. Track alteration in the Chan-hom/Nangka case was partly related to the indirect interaction conceptual model of *Carr et al*. [1997], and tracks of both Goni and Atsani were mainly determined by the environmental flow.

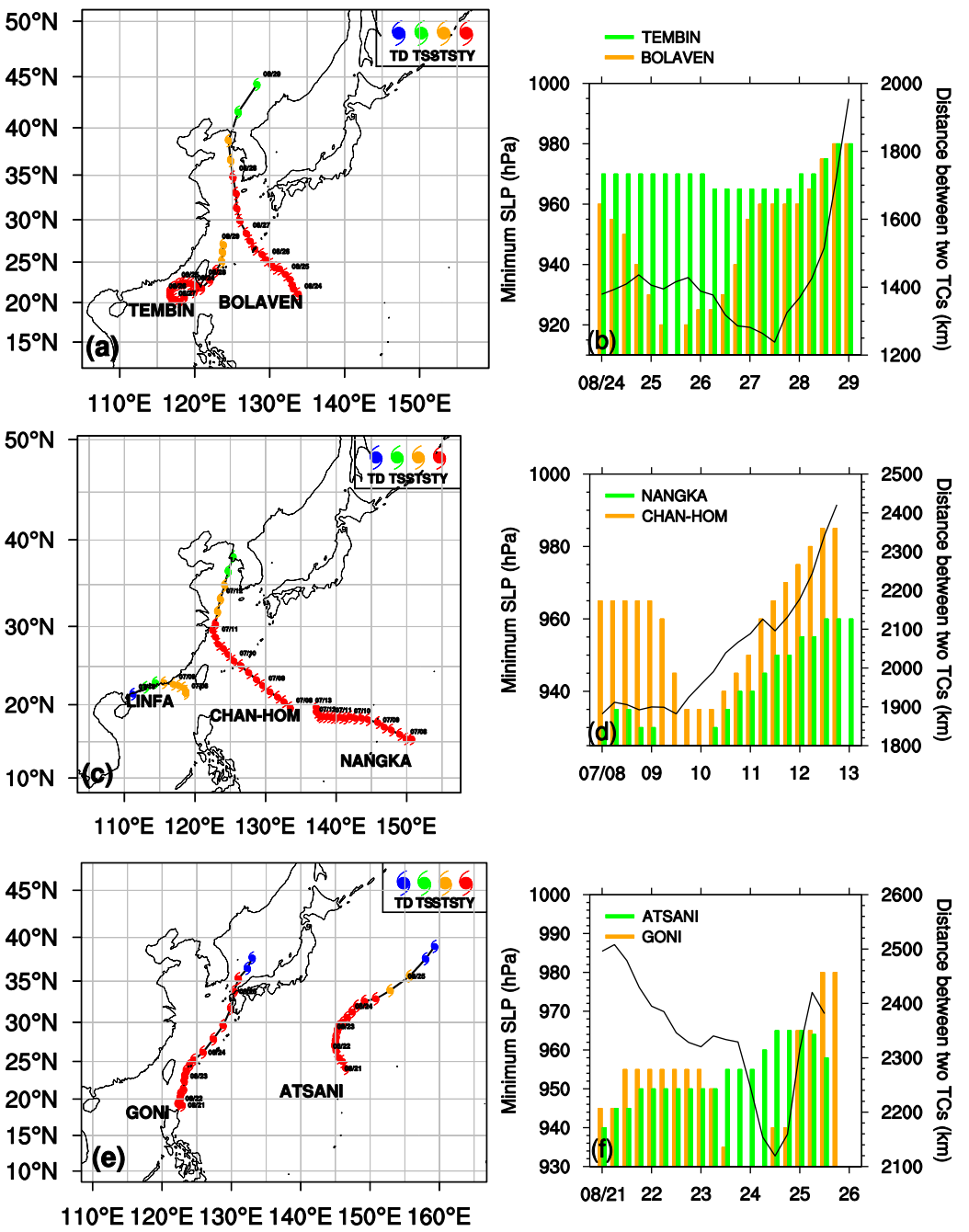

Figure 1. RSMC best tracks for TCs (a) Bolaven/Tembin, (c) Chan-hom/Nangka, and (e) Goni/Atsani. Temporal variations of minimum SLP (bar, hPa) and distance between binary TCs (solid line, km) for (b) Bolaven (orange)/Tembin (green), (d) Chan-hom (orange)/Nangka (green), and (f) Goni (orange)/Atsani (green) cases. All fields are plotted for the cycling/forecast period of each binary TC case.

3. Experimental Design

In order to investigate the effects of satellite radiance data assimilation on analyses and forecasts of binary TC cases, two data assimilation experiments are conducted for each case. In CONV experiment, conventional observations together with satellite-derived wind observations such as QuikSCAT and Atmospheric Motion Vector (AMV) are assimilated. Global Positioning System (GPS) refractivity observations from the Constellation Observing System for Meteorology Ionosphere and Climate (COSMIC) [*Liu et al.*, 2007] are also assimilated in the CONV experiment. In SAT_CONV experiment, clear-sky radiance observations as well as all

Table 1. Infrared and Microwave Instruments, Satellites on Which Instruments are Loaded, and Channels Used for Data Assimilation[a]

Instruments		Satellites	Channels	Observation Error
Infrared	HIRS	NOAA-15/16/**17/18**	2	0.70/**0.60**
			3	0.57/**0.53**
			4	0.42/**0.40**
			5	0.36/**0.36**
			6	0.46/**0.46**
			7	0.53/**0.57**
			8	1.00/**1.00**
			9	1.10/**1.10**
			10	0.55/**0.60**
			11	1.10/**1.20**
			12	1.70/**1.60**
			13	0.45/**0.36**
			14	0.25/**0.26**
			15	0.30/**0.26**
Microwave	AMSU-A	NOAA-15/**18/19, MetOp-A/B,** *EOS-Aqua*	5	0.30/**0.30**/*0.34*
			6	0.23/**0.25**/*0.40*
			7[b]	0.25/**0.27**/-
			8	0.28/**0.27**/*0.45*
			9	0.34/**0.30**/*0.40*
	AMSU-B[c]	NOAA-15/**16/17**	3	3.50/**3.50**
			4	3.20/**3.00**
			5	2.50/**2.80**
	MHS	NOAA-18/19, MetOp-A/B	3	2.50
			4	2.00
			5	2.00
	ATMS	Suomi NPP	6	0.30
			7	0.25
			8	0.27
			9	0.27
			10	0.30
			18	2.00
			19	2.00
			20	2.00
			21	2.00
			22	2.00
	SSMIS	DMSP-16	3	4.00
			4	4.00
			5	4.00
			6	4.00
			9	3.00
			10	3.00
			11	3.00

[a]Observation error standard deviations are also included. The same color (e.g., black, blue, and red) is used for the same observation error.
[b]Channel 7 of AMSU-A is excluded for MetOp-B and EOS-Aqua satellites.
[c]Observations from AMSU-B sensor are available only for Bolaven/Tembin case.

observations assimilated in the CONV experiment are assimilated. Radiance observations include High-resolution Infrared Radiation Sounder (HIRS) from NOAA-15/16/17/18 satellites, AMSU-A from NOAA-15/18/19, MetOp-A/B, and EOS-Aqua satellites, AMSU-B from NOAA-15/16/17 satellites, Microwave Humidity Sounder (MHS) from NOAA-18/19 and MetOp-A/B satellites, Advanced Technology Microwave Sounder (ATMS) from Suomi NPP satellite, and Special Sensor Microwave Imager/Sounder (SSMIS) from DMSP-16 satellite. Information on radiance observations, including a specification of observation errors is summarized in Table 1. Observation errors used in this study are from the default values specified in the WRFDA system. Radiance observation errors can be tuned using various methods such as *Desroziers and Ivanov* [2001], but that is beyond the scope of this study.

Cycled analysis-forecast experiments with a 6 h cycling interval are performed for each binary TC case. The cycling period for each case starts 5 days before one of binary TCs passes the Korean Peninsula, and it ends after 13 cycles (Table 2). The forecast length for the first cycle is 120 h and it is decreased by 6 h as the cycle goes on (i.e., 48 h forecast for the last cycle). The background for the first cycle is from the National Centers for Environmental Prediction (NCEP) Global Forecast System (GFS) analysis (0.5° resolution), afterward the background for the current cycle is the 6 h forecast starting from the analysis of the previous cycle. The lateral boundary condition for each cycle's forecast is from the corresponding NCEP GFS forecasts.

All forecasts employ the Advanced Research Weather Research and Forecasting (ARW-WRF) [*Skamarock et al*., 2008] model version 3.7.1. A single domain with a horizontal resolution of 12 km is used for each binary TC case, and the geographical area of the domain varies with the case (Figure 1). There are 45 vertical levels up to the model top at 10 hPa. The following physical parameterization schemes are used: the Kain-Fritsch cumulus parameterization scheme [*Kain*, 2004], the WRF Single Moment 6-class (WSM6) microphysics scheme [*Hong and Lim*, 2006], the Yonsei University (YSU) planetary boundary layer scheme [*Hong et al*., 2006], the

Table 2. Cycling Periods for the Bolaven/Tembin, Chan-hom/Nangka, and Goni/Atsani Binary TC Cases

Binary TC Case	Cycling Period
Bolaven/Tembin	00 UTC 24 to 00 UTC 27 August 2012
Chan-hom/Nangka	00 UTC 8 to 00 UTC 11 July 2015
Goni/Atsani	00 UTC 21 to 00 UTC 24 August 2015

Rapid Radiative Transfer Model for GCMs (RRTMG) shortwave and longwave radiation schemes [*Iacono et al*., 2008], and the Noah land surface model [*Chen and Dudhia*, 2001].

The WRFDA [*Barker et al*., 2012] system includes three/four-dimensional variational (3D-/4D-Var), ensemble transform Kalman filter (ETKF), and hybrid data assimilation methods, and in this study, the 3D-Var method within WRFDA version 3.7.1 is used. Background error covariance is calculated by using the National Meteorological Center (NMC) method [*Parrish and Derber*, 1992], where background error statistics are computed based on the differences between 24 and 12 h forecasts for a monthlong period. For each case and the corresponding computational domain, the background error covariance is computed using the forecast differences for a monthlong period, starting 1 month before the cycling period of each case. The WRFDA system has several options for background error covariance modeling, and cv5 option is used in this study. The horizontal covariance is represented by a recursive filter and the vertical covariance is modeled by an empirical orthogonal function. Control variables are stream function, unbalanced velocity potential, unbalanced temperature, unbalanced surface pressure, and pseudo relative humidity. When a temperature observation is assimilated, the impact of the observation can be spread to other variables (e.g., wind variables). However, the impact of a moisture observation is confined to a moisture variable because moisture variable is not coupled with the other variables.

An observation operator, which relates model variables to observations, for radiance observations is a radiative transfer model, and the Community Radiative Transfer Model (CRTM) [*Han et al*., 2006; *Liu and Weng*, 2006], which is one of the most commonly used radiative transfer models and developed by the Joint Center for Satellite Data Assimilation (JCSDA), within the WRFDA system is used in this study. The raw radiance data are thinned to a 60 km grid to avoid potential error correlations between adjacent observations [*Liu and Rabier*, 2002]. In previous studies on radiance DA [*Liu et al*., 2012; *Schwartz et al*., 2012; *Xu et al*., 2013; *Xu et al*., 2015], raw radiance observations are thinned to a grid with resolution of 2–6 times of a model resolution. Thinning meshes of 24, 36, 48, 60, and 72 km are tested, but no significant difference is found among meshes. Approximately, 72% of the total radiance observations are rejected by the thinning and quality control processes. Radiance observations within ± 3 h of the analysis time are assumed to be valid at the analysis time. Generally, only a subset of available channels is assimilated, and channel selection is performed based on weighting functions and known quality of a specific channel. For example, AMSU-A channels 1–4 and 15 are not assimilated because they have large sensitivities to uncertain surface parameters (e.g., emissivity and skin temperature). Channels 10–14, which have peaks in weighting functions at high altitudes, are not assimilated because of a relatively low model top (at 10 hPa). Therefore, only AMSU-A channels 5–9 are assimilated in this study, which is a default setting of the WRFDA system.

Radiance observations are prone to have systematic errors (i.e., biases), and these biases should be removed before assimilation to obtain an optimal analysis. In this study, Variational Bias Correction (VarBC) [*Derber and Wu*, 1998; *Dee*, 2004; *Auligné et al*., 2007], which includes bias correction coefficients as a part of control variables, is used for bias correction of radiance observations. In the WRFDA system, VarBC uses seven predictors: the scan position, the square and cube of scan position, 1000–300 and 200–50 hPa layer thicknesses, surface skin temperature, and total column water vapor [*Liu et al*., 2012]. To obtain a set of spun-up bias correction coefficients, offline-mode WRFDA VarBC is run over the computational domain of each case for a 1 month period (1 month before the cycling period of each case). Finally, with the spun-up bias correction coefficients as a starting point, the bias correction coefficients are updated at every cycle using all available observations.

Quality control of radiance observations should be performed before assimilation in order to assimilate only good observations. In the WRFDA system, quality control procedures for radiance observations include the following checks: (a) surface type check, which rejects all channels over mixed surface types, (b) observation geometry check, which removes pixels with large scan angles, (c) weather condition check, which removes all cloud-/precipitation-affected pixels, and (d) innovation (observation minus background) check, where radiance observation whose innovation exceeds $3\sigma_o$ (σ_o is an observation error standard deviation) is rejected.

4. Results and Discussions

4.1. Average Statistics Over All Cases

For each binary TC case, a total of 13 forecasts with varying forecast lengths (from 120 to 48 h) and initial times are made. Figure 2 shows the mean absolute errors of track, minimum SLP, and maximum wind speed

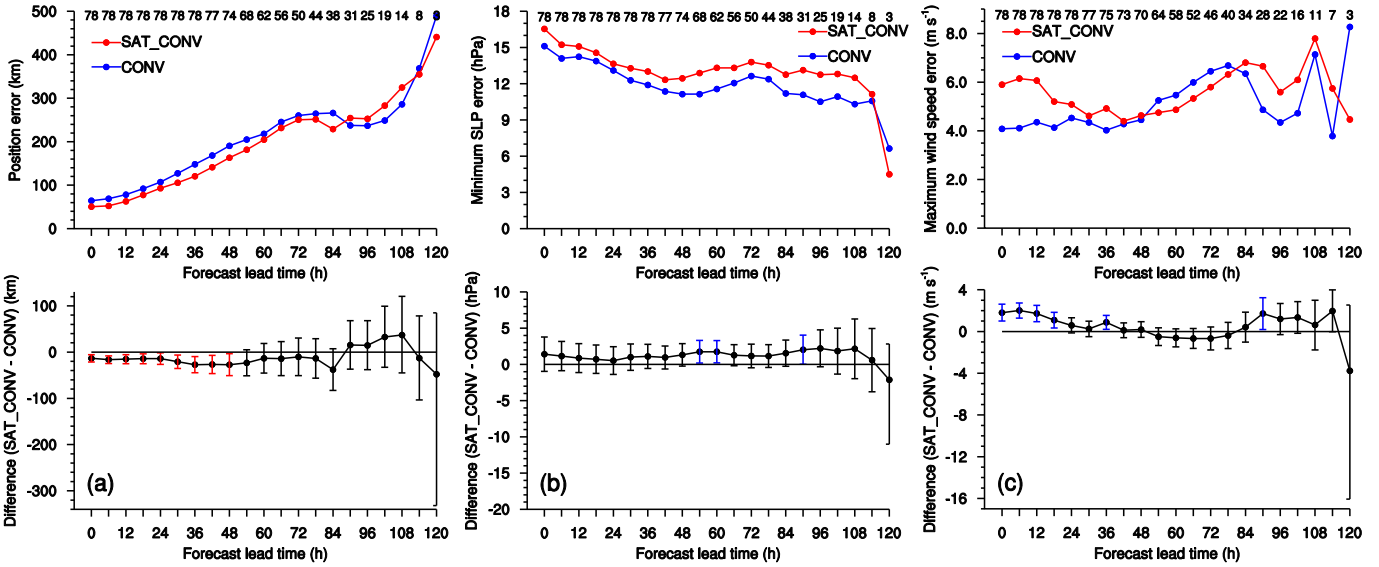

Figure 2. Mean absolute errors as a function of forecast lead time for (a) track (km), (b) minimum SLP (hPa), and (c) maximum wind speed (m s^{-1}). Blue solid lines denote results from the CONV experiment and red solid lines denote results from the SAT_CONV experiment. Number of samples used in the mean calculation for each forecast lead time is indicated at the upper portion of each figure. Differences in error between the CONV and SAT_CONV experiments for (Figure 2a) track (m), (Figure 2b) minimum SLP (hPa), and (Figure 2c) maximum wind speed (m s^{-1}) are shown. Confidence intervals at 90% confidence level are also shown. Confidence interval is colored red (blue) when the error of the SAT_CONV experiment is less (greater) than that of the CONV experiment and the difference is statistically significant.

averaged over all cases as a function of forecast lead time. Sample sizes used to calculate the mean for each forecast lead time are also shown. The 90% confidence interval for the difference in error between the CONV and SAT_CONV experiments is computed using a bootstrap resampling technique [*Hamill*, 1999; *Hamill et al.*, 2011; *Liu et al.*, 2012]. If the bounds of the confidence interval are completely below (above) zero, the error of the SAT_CONV experiment is less (greater) than that of the CONV experiment and the difference is statistically significant.

A positive impact of assimilating satellite radiances is evident in track forecasts on lead times between 0 and 84 h. The reduction in track error is statistically significant on forecast lead times of 0–48 h. It is noted that even at 0 h, track error of the SAT_CONV experiment is less than that of the CONV experiment because positive effects of radiance assimilation are accumulated through continuous cycling. Minimum SLP errors of the SAT_CONV experiment are larger than those of the CONV experiment for almost all forecast lead times, and the error differences for forecast lead times of 54, 60, and 90 h are statistically significant. The effect of assimilating satellite radiances on maximum wind speed forecasts varies with the forecast lead time. For forecast lead times of 0–48 and 84–114 h (54–78 h), maximum wind speed errors of the SAT_-CONV experiment are greater (less) than those of the CONV experiment. The error differences are statistically significant for forecast lead times of 0–18, 36, and 90 h. It should be noted that clear-sky radiances, which contain information only on the environments (not the TC itself), are assimilated, and neither initialization of vortex nor assimilation of TC position and intensity is applied in this study. Further, background error covariance is static (not flow dependent) and multivariate correlations/balances between mass and wind variables within the background error covariance used in this study are limited to those between temperature and wind variables. Because of these factors, the gain from assimilating satellite radiances is limited to the track forecasts. As a final remark, more realistic intensity forecasts can be possible by increasing the horizontal resolution of the forecast model [*Davis et al.*, 2010; *Cavallo et al.*, 2013].

Figure 3 shows the mean errors of steering winds, geopotential height, and virtual temperature averaged over all cases as a function of forecast lead time. The error difference between the CONV and SAT_CONV experiments together with its confidence interval at the 90% confidence level is also plotted. An error is defined as the root-mean-square difference (RMSD) over the entire domain between the forecast of the CONV or SAT_CONV experiment and the European Centre for Medium-Range Weather Forecasts (ECMWF) ERA Interim reanalysis. The ECMWF ERA Interim reanalysis is assumed to be good enough to be used for verification of the simulated large-scale flow because ECMWF is one of the best operational centers for TC

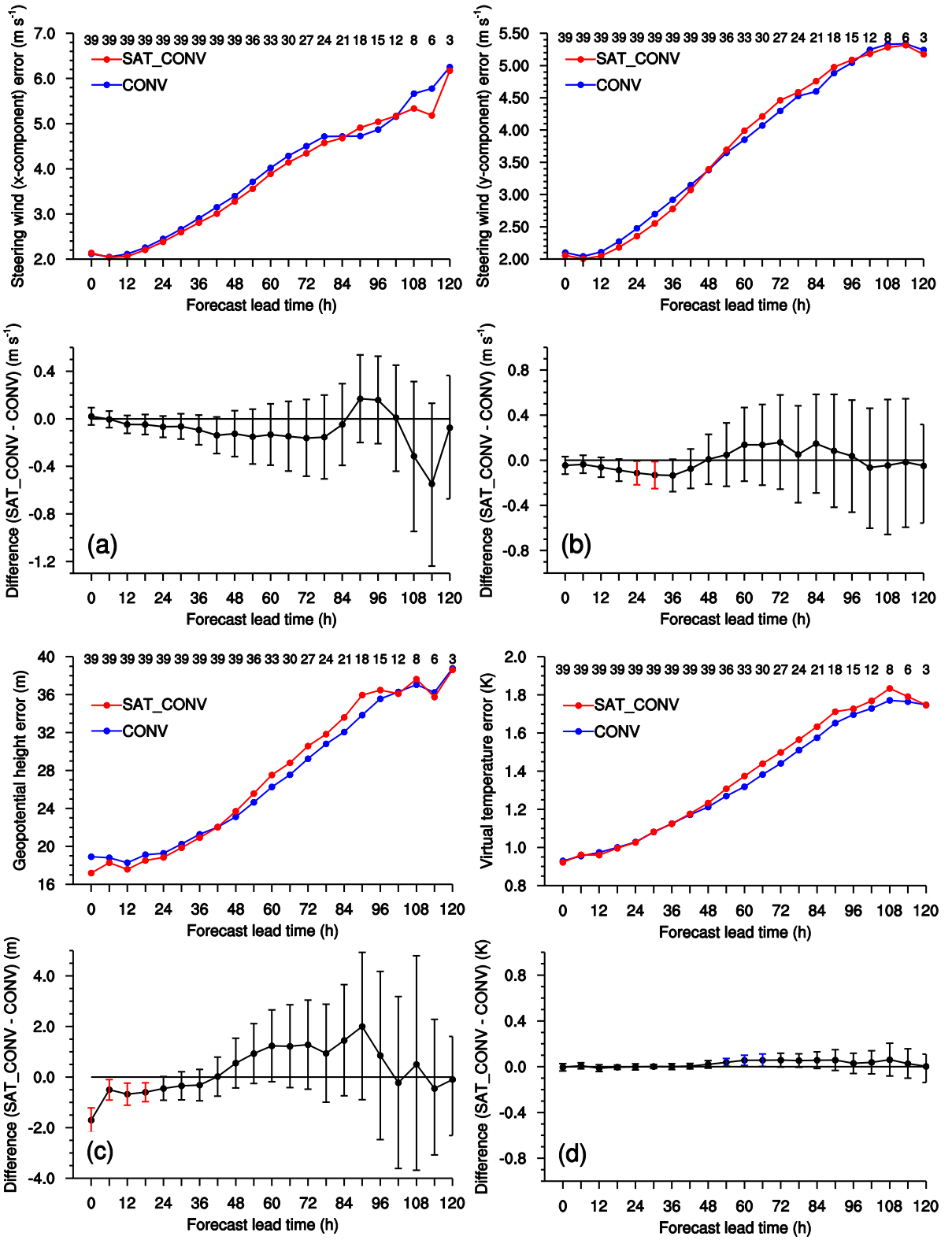

Figure 3. Mean errors as a function of forecast lead time for (a) zonal steering wind (m s^{-1}), (b) meridional steering wind (m s^{-1}), (c) geopotential height (m), and (d) virtual temperature (K). Errors are defined as root-mean-square differences between ECMWF ERA Interim reanalysis and the forecast of the CONV (blue line) or SAT_CONV (red line) experiment. Differences in error between the CONV and SAT_CONV experiments with the corresponding confidence intervals at 90% level for (Figure 3a) zonal steering wind (m s^{-1}), (Figure 3b) meridional steering wind (m s^{-1}), (Figure 3c) geopotential height (m), and (Figure 3d) virtual temperature (K) are also shown. Confidence interval is colored red (blue) when the error of the SAT_-CONV experiment is less (greater) than that of the CONV experiment and the difference is statistically significant.

track forecasts [*Fiorino*, 2009]. Steering winds are defined as a deep-layer (925–200 hPa) mean of wind fields. Zonal steering wind errors of the SAT_CONV experiment are smaller than those of the CONV experiment for almost all forecast lead times although the error differences are not statistically significant at the 90% level. Meridional steering wind errors of the SAT_CONV experiment are reduced (increased) compared with the CONV experiment for forecast lead times of 0–48 h (54–96 h). Geopotential height forecasts are improved (degraded) in the SAT_CONV experiment compared with the CONV experiment for forecast lead times of 0–42 h (48–96 h). Less geopotential height errors in the SAT_CONV experiment are statistically significant for lead times of 0–18 h. Finally, virtual temperature errors of the SAT_CONV experiment are larger than those of the CONV experiment after 48 h and the differences are statistically significant for forecast lead times of 54–66 h. Steering winds and geopotential height errors are reduced for short forecast lead times (0–48 h) through the assimilation of satellite radiances. The larger impact of assimilating temperature-sensitive and/or moisture-sensitive radiances on wind forecasts rather than temperature and/or humidity forecasts is consistent with the results of *McNally* [2007]. Although wind forecasts are improved through the background error covariance in the 3D-Var analysis and the use of the 6 h forecast from the previous cycle as the background for the current cycle, further improvements are expected by using a more advanced DA method and/or covariance model.

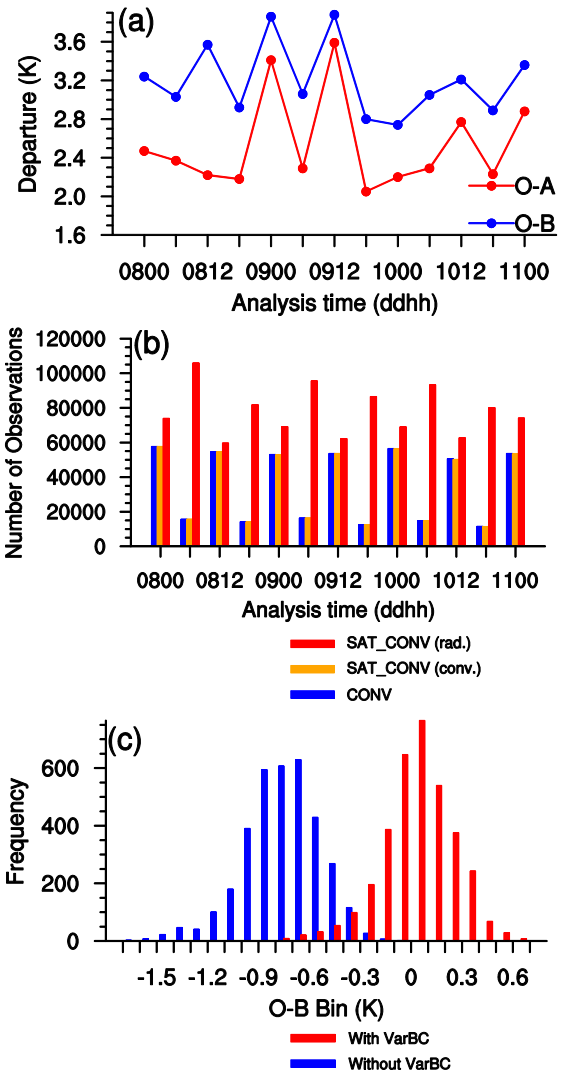

Figure 4. (a) Root-mean-square values of O-B (blue, K) and O-A (red, K) of brightness temperature for a channel 9 of SSMIS sensor on board DMSP-16 satellite, (b) number of assimilated observations for the CONV (blue) and SAT_CONV (orange and red) experiments, and (c) histogram of O-B values of brightness temperature for a channel 6 of AMSU-A sensor on board MetOp-B satellite at 00 UTC 8 July 2015 without (blue, K) and with (red, K) bias correction.

Results from the Chan-hom/Nangka and Bolaven/Tembin cases will be presented in sections 4.2 and 4.3, respectively. The effects of assimilating radiances are positive in the Goni/Atsani case but they are not as dramatic as in the Chan-hom/Nangka case. Therefore, we excluded results from the Goni/Atsani case for brevity.

4.2. Indirect Interaction Case: Chan-hom/Nangka

Figure 4 shows the root-mean-square (RMS) values of observation minus background (O-B) and observation minus analysis (O-A) for brightness temperature and the number of assimilated observations as a function of analysis time. Figure 4 also includes histogram of O-B values for brightness temperature with and without bias correction. For all analysis times (i.e., cycles), the RMS values of O-A are less than those of O-B. This implies that 3D-Var analysis is done successfully at each analysis time. The number of conventional observations assimilated in the SAT_CONV experiment is similar to that in the CONV experiment. The number of conventional (radiance) observations at 00 UTC and 12 UTC is greater (less) than that at 06 UTC and 18 UTC. Through the bias correction, a negative bias in observed brightness temperature is effectively removed.

Figure 5 shows the mean absolute track errors of the CONV and SAT_CONV experiments as a function of forecast lead time. For TC Chan-hom, the track errors of the

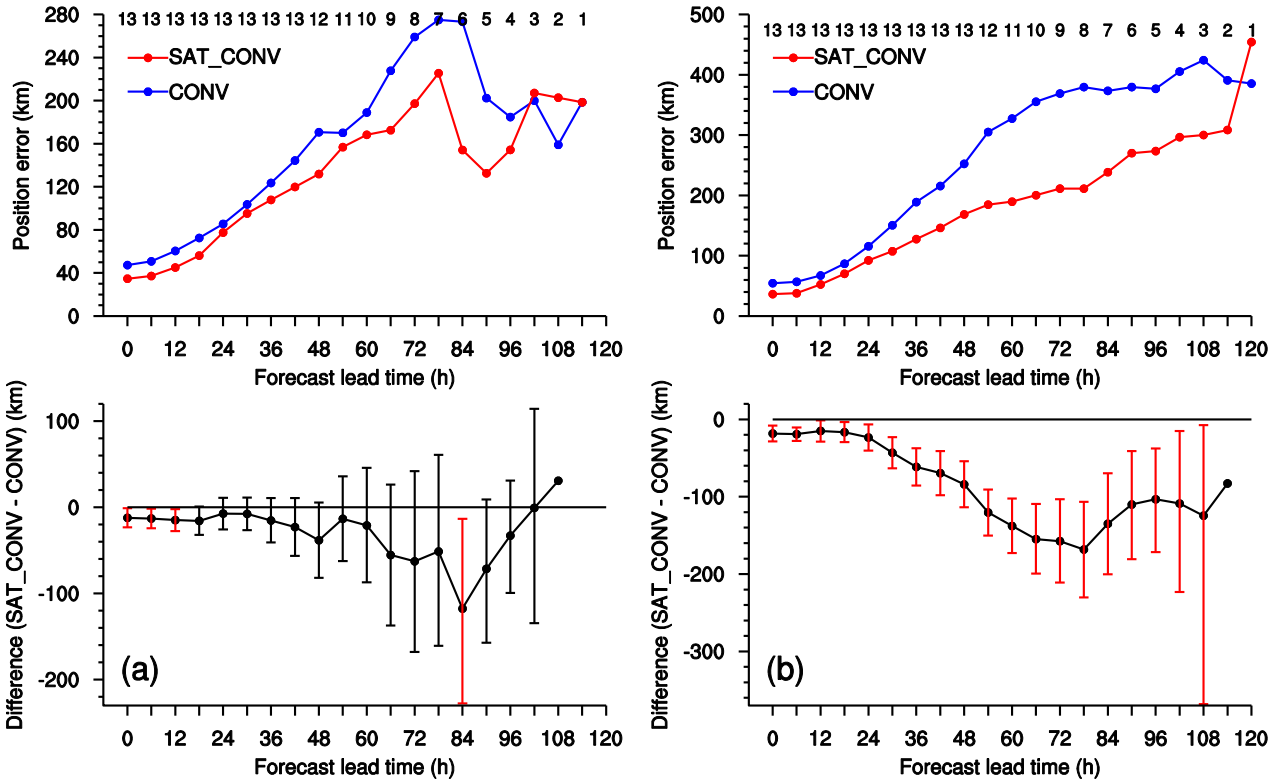

Figure 5. Mean absolute track errors (km) of the CONV (blue line) and SAT_CONV (red line) experiments as a function of forecast lead time for TC (a) Chan-hom and (b) Nangka. Differences in track error and the corresponding confidence intervals at 90% level for TC (Figure 5a) Chan-hom and (Figure 5b) Nangka are also shown. Confidence interval is colored red (blue) when the error of the SAT_CONV experiment is less (greater) than that of the CONV experiment and the difference is statistically significant.

SAT_CONV experiment are smaller than those of the CONV experiment for almost all forecast lead times. The reduction in track error is statistically significant for forecast lead times of 0–12 and 84 h. Overall, track errors of TC Nangka are larger than those of TC Chan-hom. Track errors of the SAT_CONV experiment are reduced considerably compared with the CONV experiment for nearly all forecast lead times. The track error reduction in the SAT_CONV experiment is statistically significant for all forecast lead times. Assimilating satellite radiances clearly reduces track errors of both TCs and the improvement is more substantial in the TC Nangka's forecast, where track errors in the CONV experiment are larger.

In order to figure out the reason for the improvement in track forecasts of the SAT_CONV experiment, the RMSDs of steering winds verified against ERA Interim reanalysis are computed. Figure 6 shows mean steering wind errors of the CONV and SAT_CONV experiments as a function of forecast lead time. For zonal steering wind, forecast errors of the SAT_CONV experiment are smaller than those of the CONV experiment for forecast lead times of 12–120 h. The error reduction is statistically significant for forecast lead times of 18–84 h. Although the amount of error reduction is relatively small, forecast errors of meridional steering wind of the SAT_CONV experiment are reduced compared with the CONV experiment for nearly all forecast lead times. Less meridional steering wind errors are statistically significant for forecast lead times of 54–78 h. There is no direct interaction between simulated TCs Chan-hom and Nangka. Therefore, the environmental flow plays an important role in determining tracks of both TCs. Through the assimilation of satellite radiances, the WNPSH and corresponding steering flow are simulated well in the SAT_CONV experiment, and this results in improvements in track forecasts. Note that the improvement in the initial positions in the SAT_CONV experiment through continuous cycling may contribute to track error reduction.

An error of the analysis at each cycle is defined as the difference between the analysis of the CONV or SAT_CONV experiment and ERA Interim reanalysis. The ERA Interim reanalysis is good enough to be used for verifying forecasted large-scale fields as in section 4.1. To evaluate an overall quality of the analyses of the two experiments, 850 hPa temperature and 500 hPa geopotential height errors for a total of 13 cycles are computed and they are averaged (Figure 7). Warm biases with the maximum value of about 3 K are dominant over

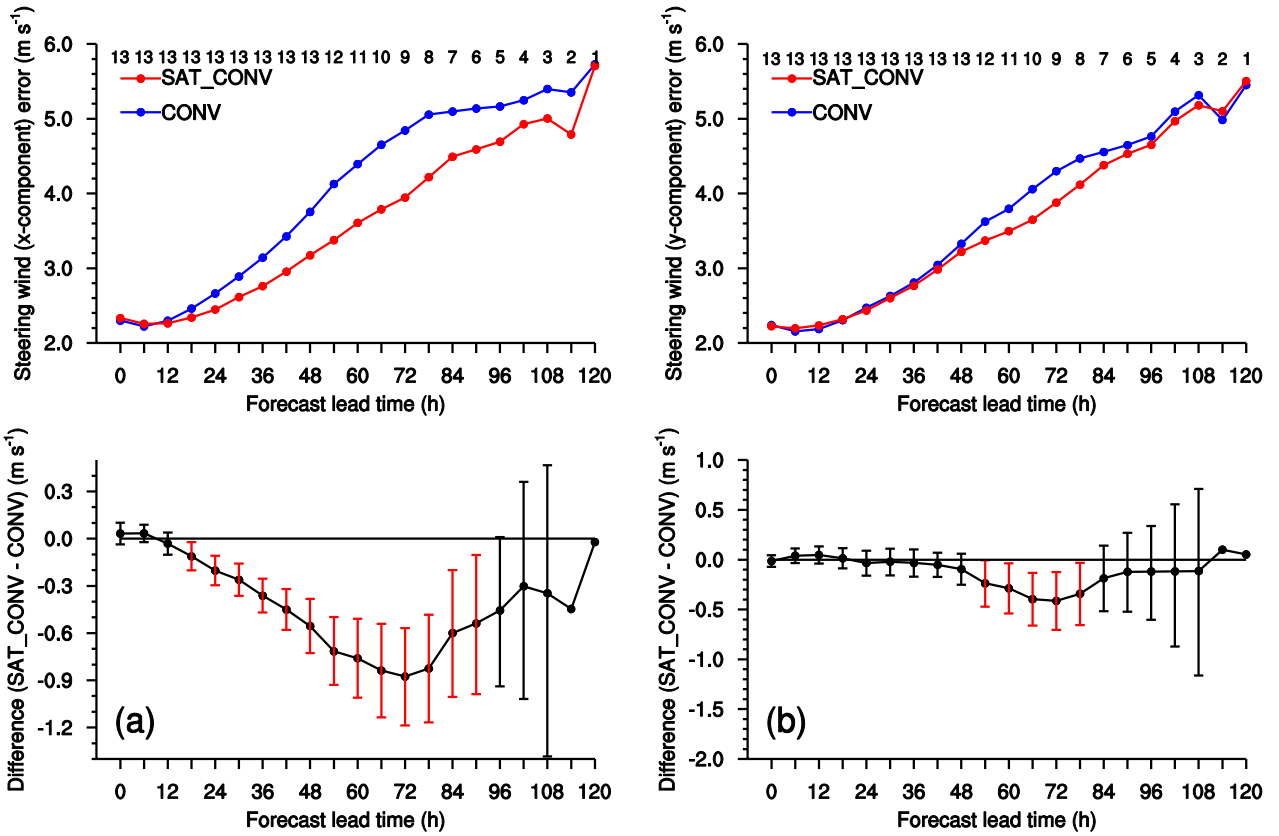

Figure 6. Mean errors of the CONV (blue line) and SAT_CONV (red line) experiments as a function of forecast lead time for (a) zonal steering wind (m s^{-1}) and (b) meridional steering wind (m s^{-1}). Differences in error between the CONV and SAT_CONV experiments with the corresponding confidence intervals at 90% level for (Figure 6a) zonal steering wind (m s^{-1}) and (Figure 6b) meridional steering wind (m s^{-1}) are also shown. Confidence interval is colored red (blue) when the error of the SAT_CONV experiment is less (greater) than that of the CONV experiment and the difference is statistically significant.

the WNP in the CONV experiment. Those warm biases are reduced in the SAT_CONV experiment, especially over the region north of 20°N. Geopotential height errors over most of the domain are positive in the CONV experiment (except along the center of each TC) and positive biases are over 40 m near the centers of two TCs. Positive biases of 500 hPa geopotential height over the WNP are consistent with the warm biases at 850 hPa. Compared with the CONV experiment, positive biases in 500 hPa geopotential height are reduced in the SAT_CONV experiment, especially near the WNPSH. Assimilating satellite radiances cools the lower atmosphere and lowers midlevel heights over the WNP. This makes the analysis of the SAT_CONV experiment closer to the ERA Interim reanalysis, and finally, contributes to the improvements in forecasts of the WNPSH, steering flow, and tracks of TCs Chan-hom and Nangka.

Figure 8 shows simulated tracks of two TCs for the CONV and SAT_CONV experiments. A total of 13 forecasted tracks with different initial times are shown, and the observed positions from the RSMC best track data are also plotted. Overall, the forecasted tracks of the SAT_CONV experiment agree more closely with the best track than those of the CONV experiment for both TCs. In the observations, Chan-hom moved northwestward until 06 UTC 11 July 2015, then it turned northeastward near 30°N, and it headed toward the Korean Peninsula. The observed northwestward movement is simulated in both experiments, but there appears a westward bias in the averaged location of turning point, especially in the CONV experiment. Although most of the simulated tracks in the SAT_CONV experiment are shifted westward compared with the observation during the northeastward movement, the slope of movement is simulated to be close to the best track. However, in the CONV experiment, the eastward component of Chan-hom's movement in most of the simulated tracks is overestimated, and this results in larger track errors than the SAT_CONV experiment. TC Nangka's best track indicates that it moved northwestward until 06 UTC 9, then it headed westward, and it turned northwestward at 00 UTC 12 July 2015. In the CONV experiment, in most cases, TC Nangka moves southwestward after the initial northwestward movement. Most of the simulated tracks in

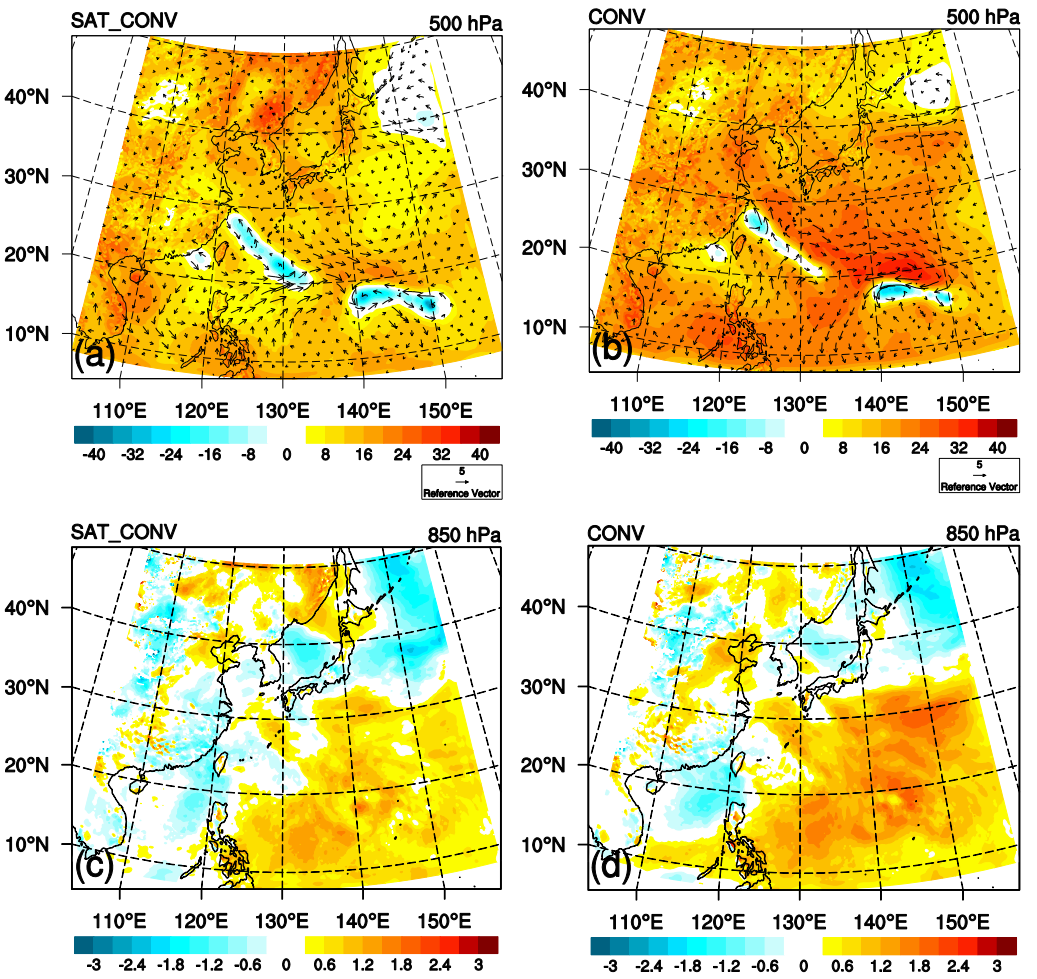

Figure 7. Averaged analysis errors of 500 hPa geopotential height (shading, m) and wind (vector, m s^{-1}) for the (a) SAT_CONV and (b) CONV experiments. Averaged analysis errors of 850 hPa temperature (shading, K) for the (c) SAT_CONV and (d) CONV experiments. An analysis error is defined as the difference between the analysis of the CONV or SAT_CONV experiment and ERA Interim reanalysis, and analysis errors over the cycling period are averaged.

the SAT_CONV experiment are similar to the best track although the simulated westward movement is too slow after 00 UTC 11 July 2015. Seventy-two hours forecasted tracks initialized at 00 UTC 10 July 2015 are selected as typical forecasts of the CONV and SAT_CONV experiments and simulated steering flows associated with these forecasts are analyzed.

Figure 9 shows the horizontal distributions of steering flow valid at 00 UTC 12 (48 h forecast) and 00 UTC 13 (72 h forecast) July 2015 for the CONV and SAT_CONV experiments. The corresponding steering-flow distributions of the ERA Interim reanalysis are also shown as a reference. At 00 UTC 12 July 2015, the WNPSH, which was located east of TC Chan-hom, caused northeastward steering flow in the ERA Interim reanalysis. Steering flow related to the WNPSH in the SAT_CONV experiment is also toward the northeast like the ERA Interim reanalysis. However, in the CONV experiment, the center of the simulated WNPSH is shifted southward compared with the reanalysis, and hence the eastward component of steering flow is overestimated. At 00 UTC 13 July 2015, the WNPSH was located north of TC Nangka, and it induced westward steering flow in the ERA Interim reanalysis. In the SAT_CONV experiment, the WNPSH and the corresponding steering flow are reasonably simulated. In contrast, the simulated WNPSH in the CONV experiment causes consistent southwestward steering flow. The WNPSH and steering flow are forecasted well in the SAT_CONV experiment, and consequently, forecasted tracks of both TCs are close to the best tracks.

In summary, tracks of TCs Chan-hom and Nangka are mainly determined by the environmental flow because there is no direct interaction between two TCs. The WNPSH and the corresponding steering flow

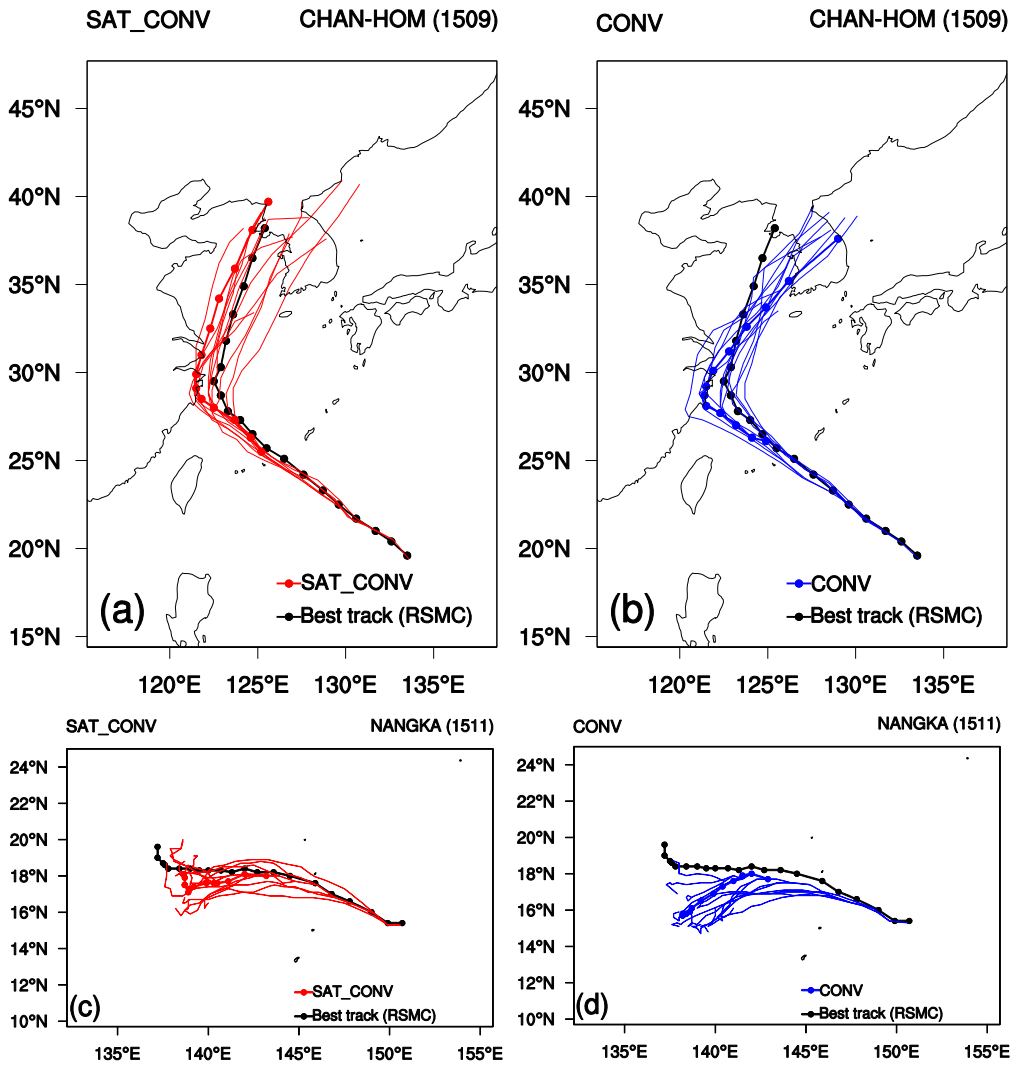

Figure 8. Forecasted tracks of TC Chan-hom for the (a) SAT_CONV (red) and (b) CONV (blue) experiments with 13 different forecast initial times and forecast lengths. Forecasted tracks of TC Nangka for the (c) SAT_CONV (red) and (d) CONV (blue) experiments. The 72 h forecasts initialized at 00 UTC 10 July 2015 are emphasized. Observed tracks (black) from the RSMC best track data are also shown.

affect the tracks of two TCs. Assimilation of satellite radiances in the SAT_CONV experiment results in improved forecasts of the WNPSH and steering flow, and finally, leads to better track forecasts. It should be noted that initial positions of two TCs in the SAT_CONV experiment are closer to the best track locations than the CONV experiment at every cycle because the 6 h forecast from the previous cycle is used as the background for the current cycle.

4.3. Direct Interaction Case: Bolaven/Tembin

For the Bolaven/Tembin case, 3D-Var analysis and bias correction are done successfully at every cycle as in the Chan-hom/Nangka case (not shown).

Figures 10a and 10b show the mean absolute track errors of the CONV and SAT_CONV experiments as a function of forecast lead time. For TC Bolaven, track errors of the SAT_CONV experiment are larger than those of the CONV experiment for almost all forecast lead times. The increased errors are statistically significant for forecast lead times of 0–90 h. It should be noted that the error difference between the two experiments is gradually increased with the forecast lead time. This implies that errors in the initial position and intensity can affect the subsequent track forecasts. For TC Tembin, track errors of the SAT_CONV experiment

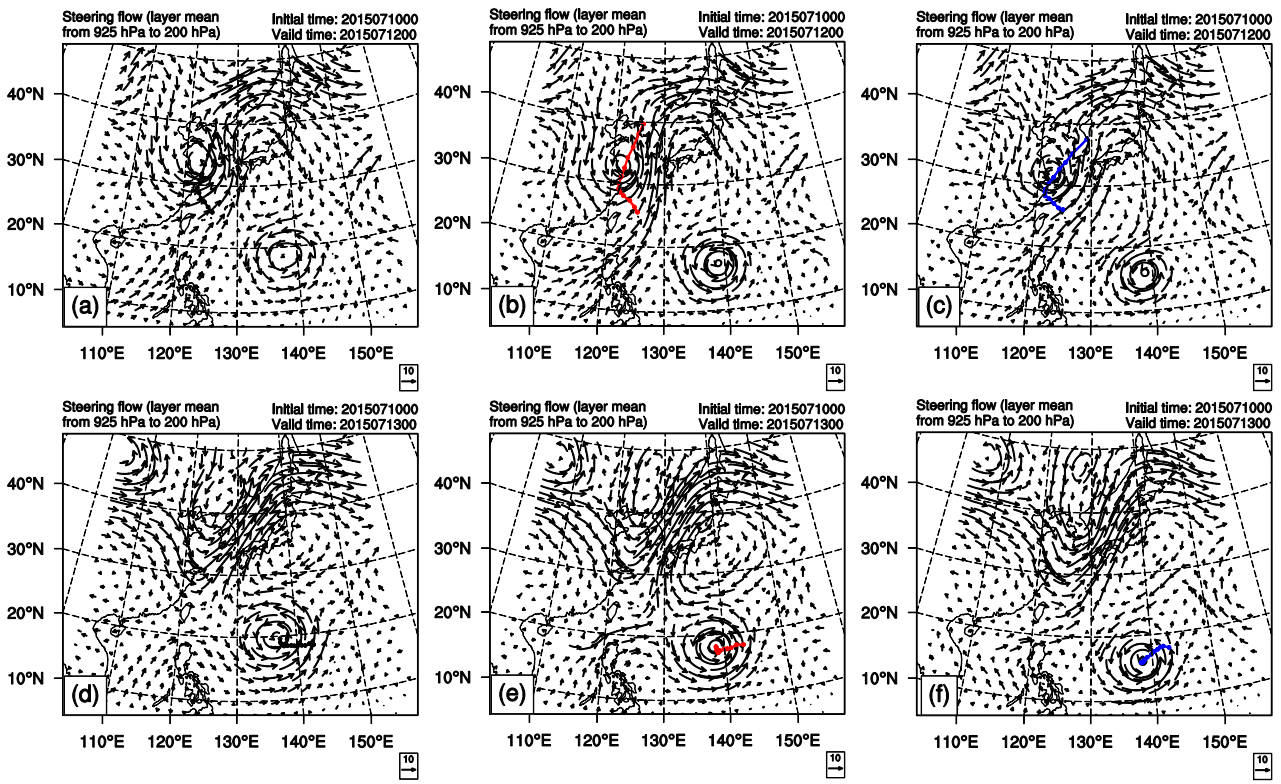

Figure 9. Horizontal distributions of steering winds at 00 UTC 12 (48 h forecast, first row) and 00 UTC 13 (72 h forecast, second row) July 2015 for the (left column) ECMWF ERA Interim reanalysis, (middle column) SAT_CONV experiment, and (right column) CONV experiment. Both the CONV and SAT_CONV experiments are initialized at 00 UTC 10 July 2015. Forecasted tracks of TCs (first row) Chan-hom and (second row) Nangka for the SAT_CONV (red) and CONV (blue) experiments together with the best tracks (black) are also shown.

are less than those of the CONV experiment for forecast lead times of 0–60 h, and the error reduction is statistically significant for lead times of 0–42 h. However, for forecast lead times of 72–108 h, track errors of the SAT_CONV experiment are increased compared with the CONV experiment, and the difference is statistically significant for lead times of 90–96 h. When the forecast initial time is near the end of the direct interaction (i.e., for later cycles with shorter forecast lengths), track errors can be reduced through the assimilation of satellite radiances. This explains less track errors of TC Tembin of the SAT_CONV experiment for shorter forecast lead times.

Figure 10c shows the averaged total track errors and initial position errors of the CONV and SAT_CONV experiments as a function of forecast initial time (i.e., for every cycle). For each cycle, track errors of TCs Bolaven and Tembin are calculated every 6 h and they are averaged. From 06 UTC 24 to 06 UTC 25 August 2012, total track errors of the SAT_CONV experiment are larger than those of the CONV experiment. During the same period, initial position errors of the SAT_CONV experiment are greater than those of the CONV experiment (except at 06 UTC 24 August 2012). After 12 UTC 25 August 2012, the reverse applies. In other words, both total track errors and initial position errors of the SAT_CONV experiment are smaller than those of the CONV experiment (except the initial position error at 18 UTC 25 August 2012). We hypothesized that the main factors for determining tracks of two TCs are the direct interaction for the period of 06 UTC 24 to 12 UTC 25 August 2012 and the environmental flow after 12 UTC 25 August 2012, respectively. There still existed a direct interaction until 12 UTC 27, but the degree of interaction was the strongest at 12 UTC 25 August 2012 when the difference of minimum SLP between the two TCs was the largest.

We divided the whole cycling period into two subperiods according to the main factor for determining tracks of two TCs: P1 is from 06 UTC 24 to 12 UTC 25 August 2012 and P2 is from 18 UTC 25 to 00 UTC 27 August 2012. Figures 11a–11d show forecasted tracks of the CONV and SAT_CONV experiments together with the best track for the two subperiods. The 120 h forecasted tracks of the CONV and SAT_CONV experiments, initialized at 00 UTC 24 August 2012, with the corresponding best track are also shown (Figures 11e

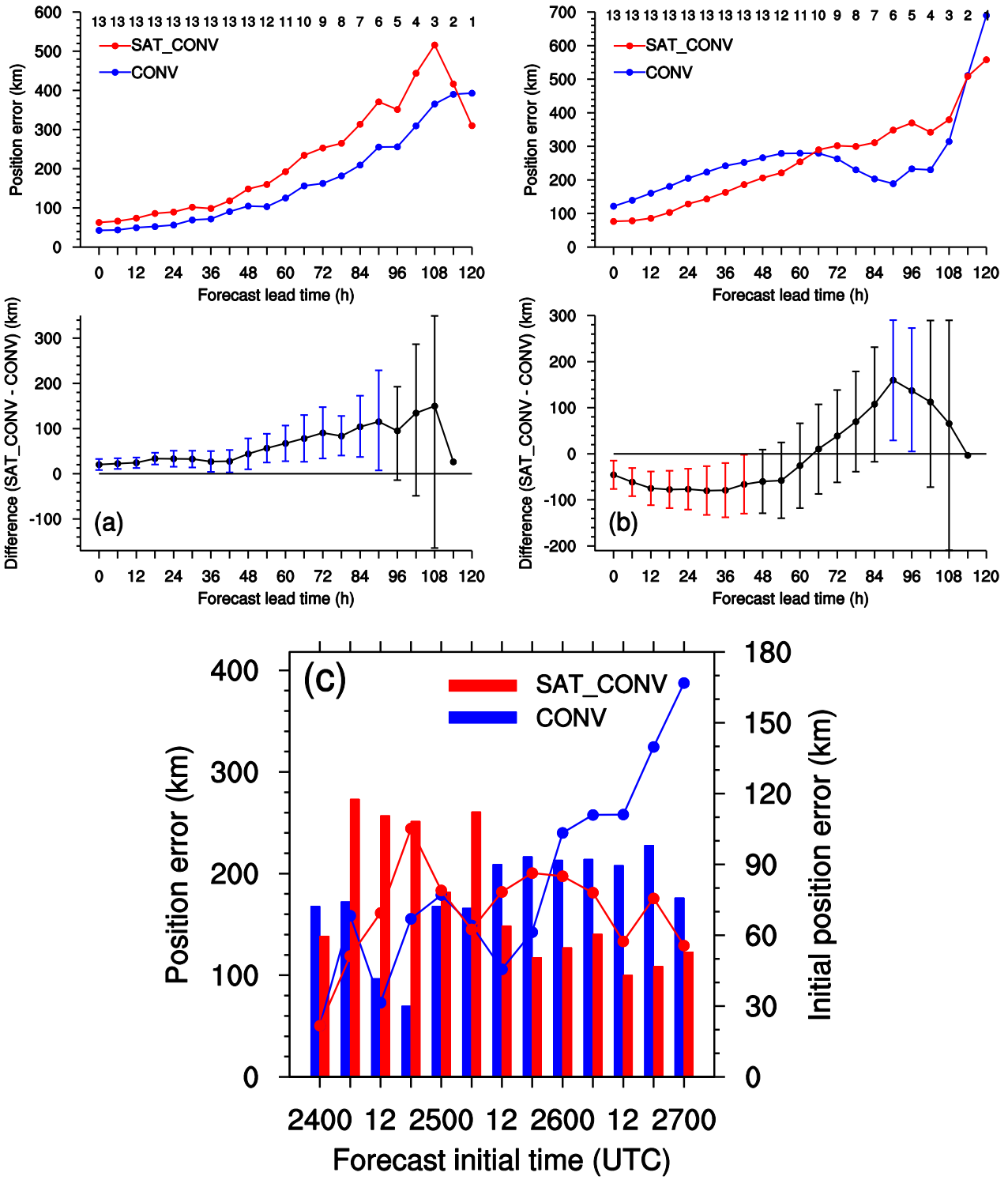

Figure 10. (a, b) Same as Figure 5 except for TC (a) Bolaven and (b) Tembin. (c) Averaged total track errors (bar, km) and initial position errors (solid line, km) of the CONV (blue) and SAT_CONV (red) experiments as a function of forecast initial time. For each cycle, track errors of TCs Bolaven and Tembin are calculated every 6 h and they are averaged to derive the averaged total track error.

and 11f). During the P1 period, most of forecasted tracks in both experiments have westward biases compared with the observations (Figures 11a and 11b). Among the forecasts within the P1 period, 114 h forecast initialized at 06 UTC 24 (emphasized with bold lines) will be analyzed in detail because forecasts of the

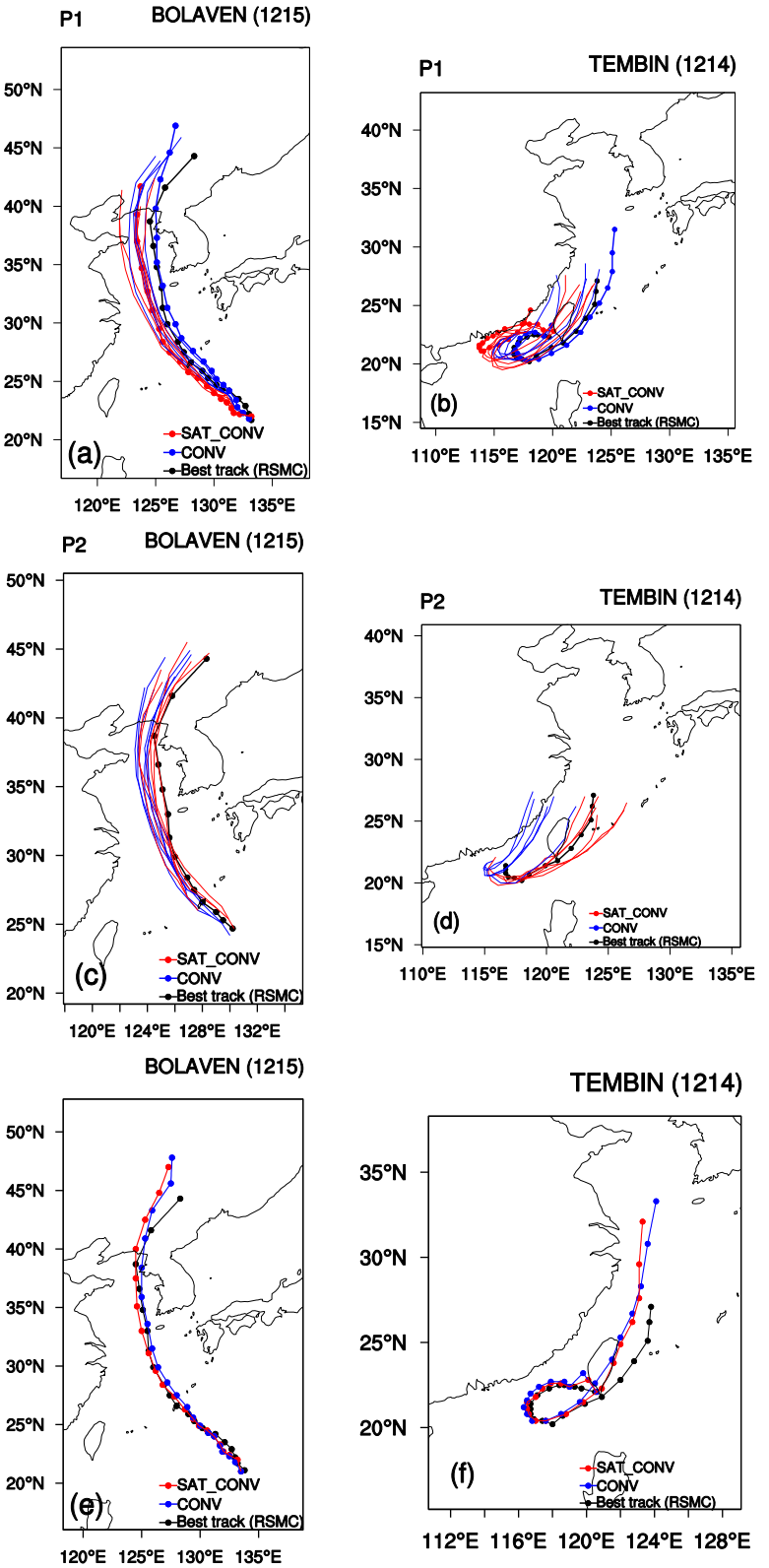

Figure 11. Forecasted tracks of the SAT_CONV (red) and CONV (blue) experiments during the P1 period for TC (a) Bolaven and (b) Tembin. Forecasted tracks of the SAT_CONV (red) and CONV (blue) experiments during the P2 period for TC (c) Bolaven and (d) Tembin. The 114 h forecast initialized at 06 UTC 24 August 2012 is emphasized. The 120 h forecasted tracks of the SAT_CONV (red) and CONV (blue) experiments for TC (e) Bolaven and (f) Tembin. Observed tracks (black) from the RSMC best track data are also shown.

CONV and SAT_CONV experiments initialized at/after 06 UTC 24 August 2012 are different from each other. From 06 UTC 24 to 12 UTC 27 August 2012 (i.e., direct-interaction period), the simulated track for TC Bolaven in the CONV experiment is slightly shifted eastward compared with the best track. In contrast, the simulated track in the SAT_CONV experiment has the consistent westward bias. After 12 UTC 27, an observed reverse-oriented monsoon trough formation is well simulated in both experiments (not shown), however, there still exists the westward bias in the SAT_CONV experiment because of the errors during the direct-interaction period (Figure 11a). Although the observed cyclonic rotation of TC Tembin during the direct-interaction period is simulated in both experiments, the length of the semimajor axis of the simulated elliptic loop is larger than the observation in the SAT_CONV experiment. After the direct-interaction period, track of TC Tembin is determined by the reverse-oriented monsoon trough formation as in the case of TC Bolaven, which is simulated in both experiments, but tracks of the SAT_CONV experiment still have westward biases because of the errors during the interaction period (Figure 11b).

During the P2 period, forecasted tracks of TC Bolaven in both experiments still have left-of-track biases, but the biases are reduced as the forecast initial time approaches the end of the direct-interaction period, especially in the SAT_CONV experiment (Figure 11c). Forecasted tracks of TC Tembin in the CONV experiment have westward biases compared with the observations. In contrast, forecasted tracks in the SAT_CONV experiment are close to the best track (Figure 11d). The 120 h forecasted tracks of TCs Bolaven and Tembin are similar to the best tracks in both experiments (Figures 11e and 11f) and this forecast will be compared with the 114 h forecast in the following analyses.

In order to find out the reason for the forecast degradation during the P1 period in the SAT_CONV experiment, the analysis and subsequent 1 day forecast differences between the CONV and SAT_CONV experiments (SAT_CONV minus CONV) are averaged over the P1 period. Midlevel (vertical average between 400 and 600 hPa) equivalent potential temperature differences between the two experiments are shown in Figure 12a. In the vicinity of the center of TC Tembin, the air at midlevels in the SAT_CONV experiment becomes colder and drier than the CONV experiment as a result of continuous cycling. On the contrary, near the center of TC Bolaven, the atmosphere between 400 and 600 hPa in the SAT_CONV experiment becomes warmer and moister than the CONV experiment. Under these conditions, the deepening rate of the simulated TC Tembin (Bolaven) can be reduced (enhanced) in the SAT_CONV experiment compared with the CONV experiment. Only clear-sky radiances are assimilated, and static (not flow-dependent) background error covariance is used in the 3D-Var analysis. Radiance observations outside a TC can affect the TC and its vicinity only through the static background error covariance, which cannot reflect the flow inside/near the TC. Note that the change in minimum SLP of TC Bolaven (Tembin) during the P1 period was decreasing (nearly constant) in the observations.

Figures 12b and 12c show the averaged errors in analysis of the CONV and SAT_CONV experiments verified against the ERA Interim reanalysis. Geopotential height errors at 500 hPa over the whole cycling period are averaged. Large geopotential height errors over the WNP and Shandong Peninsula in the CONV experiment are reduced in the SAT_CONV experiment. Synoptic environments in the SAT_CONV experiment are improved through assimilating satellite radiances as in the Chan-hom/Nangka case, and this improvement contributes to the reduced track errors of both TCs during the P2 period, when the environmental flow plays a dominant role in determining tracks of the two TCs.

In many previous studies, a centroid-relative motion approach has been used to analyze a binary interaction between two TCs. Figure 13 shows centroid-relative tracks of TCs Bolaven and Tembin for the 114 and 120 h forecasts. Simulated tracks of the CONV and SAT_CONV experiments together with the best tracks are shown. Observed centroid-relative motions of TCs Bolaven and Tembin (2012) are similar to those for TCs Nina and Ora (1978), one of the binary TCs presented in *Lander and Holland* [1993]. Further, the observed centroid-relative motions correspond well to the binary interaction model (i.e., approach, capture, cyclonic orbit, and merger/escape) suggested by *Lander and Holland* [1993]. The centroid-relative tracks computed from the 120 h forecasts are close to the best track. This implies that the direct interaction is reasonably simulated in both experiments. This also applies to the centroid-relative track from the 114 h forecast of the CONV experiment. In contrast, the centroid-relative track computed from the 114 h forecast of the SAT_CONV experiment is different from the best track. The radius of the simulated cyclonic orbit in the SAT_CONV experiment is greater than that in the observation.

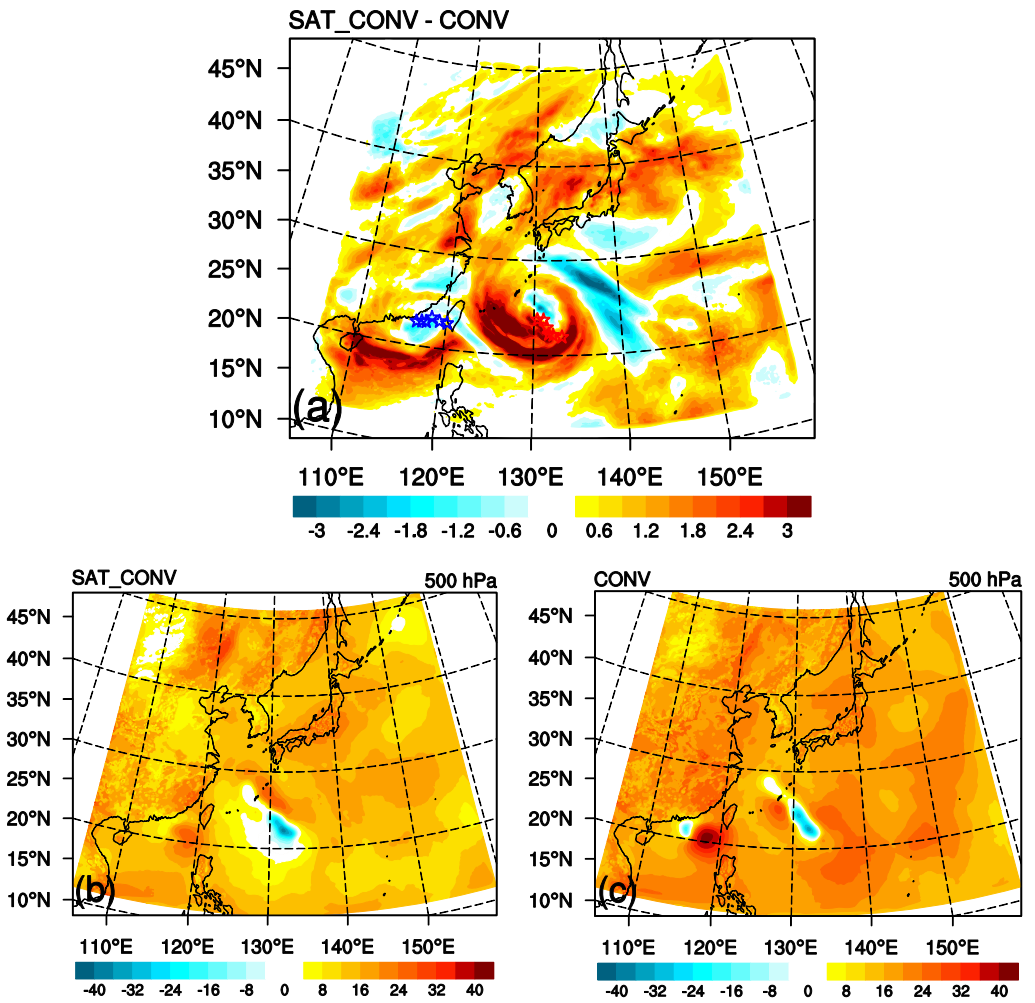

Figure 12. (a) Difference (SAT_CONV minus CONV) between the CONV and SAT_CONV experiments of the analysis and subsequent 1 day forecast of midlevel (vertical average between 400 and 600 hPa) equivalent potential temperature (shading, K). The differences during the P1 period are averaged. Positions of the simulated TCs Bolaven (red star) and Tembin (blue star) in the SAT_CONV experiment during the P1 period are also shown. Averaged analysis errors of 500 hPa geopotential height (shading, m) for the (b) SAT_CONV and (c) CONV experiments.

Figure 14 shows minimum SLP variations of TCs Bolaven and Tembin, and temporal variations of the minimum SLP difference between the two TCs (Tembin minus Bolaven) for the 114 and 120 h forecasts. Forecasts of the CONV and SAT_CONV experiments together with the observed minimum SLP from the best track data are shown. Concerning the 120 h forecast, there is little difference between the simulated minimum SLP fields of the CONV and SAT_CONV experiments. Although the individual forecasts of minimum SLP are different from the best tracks, the temporal variation of the minimum SLP difference is reasonably simulated in both experiments. Concerning the 114 h forecast, although the observed TC Bolaven's deepening between 06 UTC 24 and 12 UTC 25 and weakening between 12 UTC 25 and 00 UTC 27 are qualitatively simulated in both experiments as for the 120 h forecast, the simulated deepening rate in the SAT_CONV experiment is slightly greater than the CONV experiment. The simulated minimum SLP of TC Tembin is continuously decreasing in both experiments as for the 120 h forecast, but the simulated deepening rate of the SAT_CONV experiment is much less than that of the CONV experiment. As a result, the simulated minimum SLP difference in the SAT_CONV experiment is greater than the best track. In other words, the intensity difference between a weaker TC Tembin and a stronger TC Bolaven is overestimated in the SAT_CONV experiment.

The degree of direct interaction between binary TCs depends on the distance between two TCs, sizes of two TCs, and the intensity difference between two TCs. In both experiments, the distance between TCs

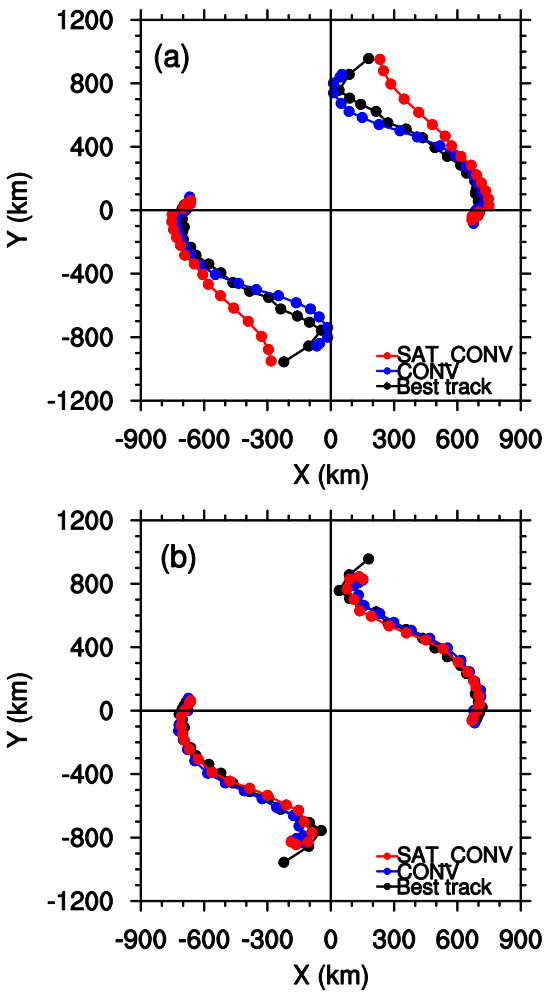

Figure 13. Centroid-relative tracks of the observation (black), CONV (blue), and SAT_CONV (red) experiments for TCs Bolaven and Tembin: (a) 114 h forecast and (b) 120 h forecast.

Bolaven and Tembin and the sizes of the two TCs are reasonably simulated (not shown). During the P1 period (e.g., 114 h forecast), the minimum SLP difference in both experiments (especially in the SAT_CONV experiment) is overestimated compared with the best track. The greater minimum SLP difference results in a too strong interaction between the two TCs. The stronger interaction simulated in both experiments leads to the westward bias of TC Bolaven's track forecast, the longer semimajor axis of TC Tembin's elliptic loop, and the greater radius of the centroid-relative tracks of both TCs. The relationship between the radius of centroid-relative track and the intensity difference between binary TCs observed in this study is consistent with *Wang and Holland* [1995]. In summary, assimilating satellite radiances can be detrimental to the track forecasts of binary TCs when the direct interaction is a main factor for determining tracks of the binary TCs.

5. Summary and Conclusions

A total of three binary TC cases, which affected the Korean Peninsula or the surrounding areas during the period of 2010–2015, were selected in this study. Two experiments are conducted for each binary TC case to investigate the effects of satellite radiance assimilation on the binary TCs' track forecasts: the CONV and SAT_CONV experiments. In the CONV experiment, all conventional observations together with satellite-derived wind and GPS refractivity observations are assimilated using the 3D-Var method. All observations assimilated in the CONV experiment plus radiance observations are assimilated in the SAT_CONV experiment. For each case, cycled analysis-forecast experiments with a cycling interval of 6 h are performed, and a total of 13 forecasts with varying forecast lengths are made. In order to assimilate radiance observations, the CRTM is used as an observation operator, various quality control procedures are performed to select good observations, and VarBC is applied to raw radiance observations to remove biases. Additionally, thinning of the original radiance observations and channel selection are carried out.

In the Chan-hom/Nangka case, there was no direct interaction between two TCs, and the positions of two TCs and the WNPSH were similar to the indirect interaction model of *Carr et al.* [1997]. Therefore, tracks of two TCs were determined by the WNPSH and the corresponding environmental flow. Through the assimilation of radiance observations in the SAT_CONV experiment, both the steering wind and track errors are reduced compared with the CONV experiment. In the Goni/Atsani case, the distance between two TCs was more than 2000 km, and hence tracks of two TCs were influenced by midlevel trough/ridge patterns and the corresponding environmental flow. Although the positive effects of assimilating radiances are not dramatic as in the Chan-hom/Nangka case, the environmental flow and tracks of both TCs are better simulated in the SAT_CONV experiment (not shown). In the Bolaven/Tembin case, there was a direct interaction between two TCs, and after the direct interaction, a reverse-oriented monsoon trough formed. During the P1 period, when the main factor determining tracks of two TCs is the direct interaction, the minimum SLP difference between two TCs is overestimated in both experiments, especially in the SAT_CONV experiment, because of the static (not flow-dependent) background error covariance used in the analysis. This leads to

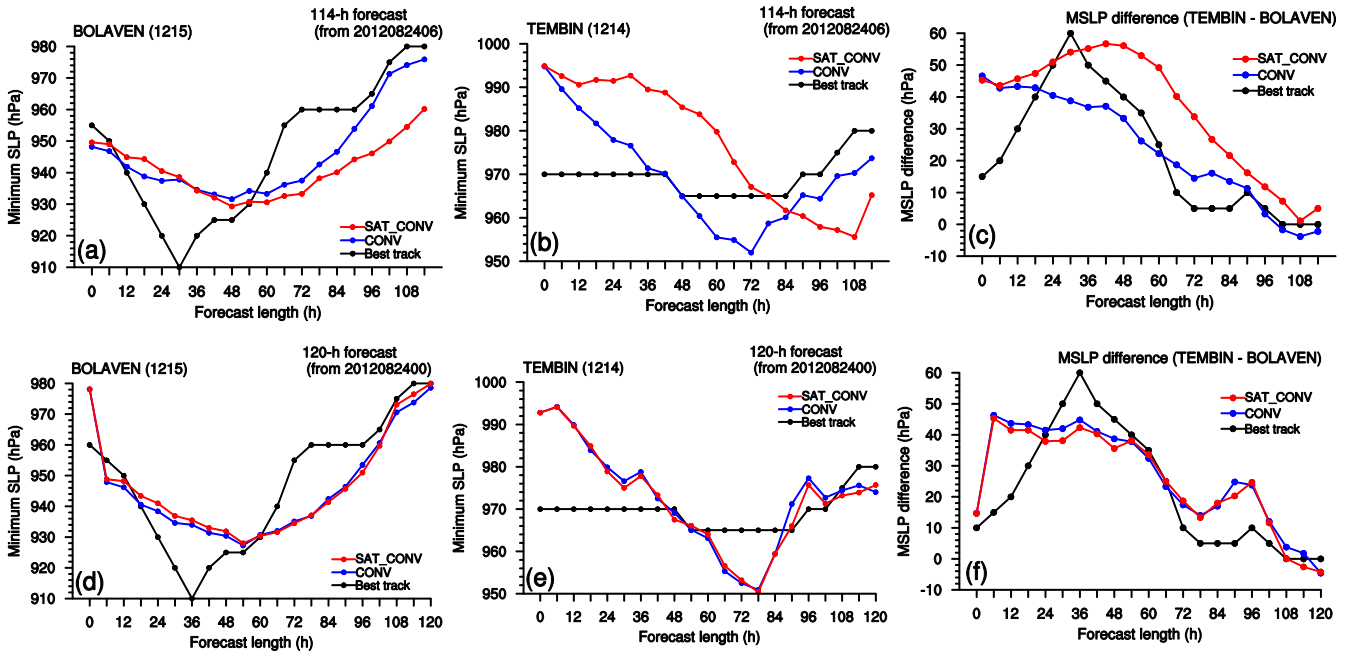

Figure 14. Temporal variations of minimum SLP (hPa) for TCs Bolaven and Tembin, and minimum SLP difference (hPa) between TCs Bolaven and Tembin (Tembin minus Bolaven). Black solid lines denote best track data, and blue (red) solid lines denote results from the CONV (SAT_CONV) experiment. Results for (a–c) 114 h forecasts and (d–f) 120 h forecasts are shown.

too strong interaction between the two TCs, and finally, track errors of both TCs are increased, especially in the SAT_CONV experiment. However, during the P2 period, when tracks of two TCs are mainly determined by the environmental flow, track errors are reduced in the SAT_CONV experiment compared with the CONV experiment through the assimilation of radiance observations. In conclusion, assimilating radiance observations can improve track forecasts of binary TCs through better simulating the environmental flow when the direct interaction is not the main factor for determining tracks of binary TCs.

In this study, only binary TC cases, which occur over the Pacific Ocean and affect the Korean Peninsula, are considered. To generalize the conclusions of this study, more binary TC cases such as ones over the Atlantic Ocean or ones not affecting the Korean Peninsula should be considered. Cloud-affected (infrared) or precipitation-affected (microwave) radiances are not assimilated in this study. Assimilating all-sky radiances can provide information not only on the environment of a TC but also on the TC itself, and hence it will significantly improve the track and intensity forecasts of binary TCs. Alternatively, initialization of TC vortex or assimilation of TC position/intensity can improve track and intensity forecasts of binary TCs even when a direct interaction between binary TCs occurs.

In this study, the 3D-Var method and corresponding static (i.e., time-invariant) background error covariance are used for assimilating satellite radiances. In the cv5 option (used in this study), there are multivariate correlations/balances between temperature and wind (and surface pressure) variables, but humidity variable is not coupled with the other variables. Satellite radiance observations contain information only on temperature and moisture of the atmosphere, and hence the use of more advanced DA methods will enable the analysis to extract more information about the steering wind through the advanced background error covariance, which has flow dependency and more appropriate multivariate correlations/balances. It should be noted that there is room for improvements in settings of radiance assimilation within the 3D-Var. Optimization of observation errors, use of different thinning methods, and identifying/filtering of harmful observations can be considered and they will be tested in a follow-up study.

In some previous studies, additional assimilation of storm position and intensity [*Liu et al.*, 2012], combined use of vortex initialization and data assimilation [*Zhang et al.*, 2012], and utilization of more advanced DA methods [*Liu et al.*, 2012; *Schwartz et al.*, 2012; *Xu et al.*, 2016] have shown potential for improving TC intensity forecasts. In a future study, the dynamic initialization method proposed by *Cha and Wang* [2013] will be

applied to binary TC cases, together with satellite radiance assimilation. In addition, more binary TC cases will be tested to obtain the robustness of conclusions of this study, and more advanced DA techniques (e.g., EnKF, hybrid) will be tested for assimilating all-sky/clear-sky satellite radiances.

Acknowledgments

The authors are thankful to the Editor-in-Chief (Robert Pincus), Associate Editor (Dick Dee), and two anonymous reviewers for their valuable comments and suggestions. This work has been supported by Korea Institute of Science and Technology Information, with the project of "Construction of HPC-based Service Infrastructure Responding to National Scale Disaster (K-17-L03-C03)". This work was also supported by the National Institute of Supercomputing and Network/Korea Institute of Science and Technology Information with supercomputing resources including technical support (KSC-2015-C2-005). The authors are grateful to Chris Snyder for fruitful discussions. The NCEP GFS analysis and forecast data are available from the National Oceanic and Atmospheric Administration (NOAA) National Operational Model Archive and Distribution System (NOMADS) web site (http://nomads.ncdc.noaa.gov/cgi-bin/ncdc-ui/define-collection.pl?model_sys=gfs4&model_name-gfs&grid_name=4). All observational data including conventional, satellite-derived wind, GPS refractivity, and satellite radiance observations can be freely obtained from the NOAA NOMADS web site (http://nomads.ncdc.noaa.gov/cgi-bin/ncdc-ui/define-collection.pl?model_sys=g-das&model_name=gdas&grid_name=999). The RSMC best track data and the ECMWF ERA Interim reanalysis data are available from the RSMC Tokyo typhoon center (http://www.jma.go.jp/jma/jma-eng/jma-center/rsmc-hp-pub-eg/besttrack.html) and the ECMWF (http://apps.ecmwf.int/datasets) web sites, respectively.

References

Auligné, T., A. P. McNally, and D. P. Dee (2007), Adaptive bias correction for satellite data in a numerical weather prediction system, *Quart. J. R. Meteorol. Soc.*, *133*, 631–642.

Barker, D., et al. (2012), The Weather Research and Forecasting Model's Community Variational/Ensemble Data Assimilation System: WRFDA, *Bull. Am. Meteorol. Soc.*, *93*, 831–843.

Bauer, P., et al. (2011), Satellite cloud and precipitation assimilation at operational NWP centres, *Quart. J. R. Meteorol. Soc.*, *137*, 1934–1951.

Bonavita, M., E. Hólm, L. Isaksen, and M. Fisher (2015), The evolution of the ECMWF hybrid data assimilation system, *Quart. J. R. Meteorol. Soc.*, *142*, 287–303.

Brand, S. (1970), Interaction of binary tropical cyclones of the western North Pacific Ocean, *J. Appl. Meteorol.*, *9*, 433–441.

Cardinali, C. (2009), Monitoring the observation impact on the short-range forecast, *Quart. J. R. Meteorol. Soc.*, *135*, 239–250.

Carr, L. E., III, M. A. Boother, and R. L. Elsberry (1997), Observational evidence for alternate modes of track-altering binary tropical cyclone scenarios, *Mon. Weather Rev.*, *125*, 2094–2111.

Cavallo, S. M., R. D. Torn, C. Snyder, C. Davis, W. Wang, and J. Done (2013), Evaluation of the Advanced Hurricane WRF data assimilation system for the 2009 Atlantic hurricane season, *Mon. Weather Rev.*, *141*, 523–541.

Cha, D.-H., and Y. Wang (2013), A dynamic initialization scheme for real-time forecasts of tropical cyclones using the WRF model, *Mon. Weather Rev.*, *141*, 964–986.

Chang, S. W.-J. (1983), A numerical study of the interaction between two tropical cyclones, *Mon. Weather Rev.*, *111*, 1806–1817.

Chen, F., and J. Dudhia (2001), Coupling an advanced land-surface/hydrology model with the Penn State/NCAR MM5 modeling system. Part I: Model description and implementation, *Mon. Weather Rev.*, *129*, 569–585.

Chen, S.-H., F. Vandenberghe, G. W. Petty, and J. F. Bresch (2004), Application of SSM/I satellite data to a hurricane simulation, *Quart. J. R. Meteorol. Soc.*, *130*, 801–825.

Davis, C., W. Wang, J. Dudhia, and R. Torn (2010), Does increased horizontal resolution improve hurricane wind forecasts?, *Weather Forecasting*, *25*, 1826–1841.

Dee, D. P. (2004), Variational bias correction of radiance data in the ECMWF system, in *Proceedings of the Workshop on Assimilation of High-Spectral-Resolution Sounders in NWP*, pp. 97–112, Eur. Cent. for Medium-Range Weather Forecasts, Reading, U. K.

DeMaria, M., and J. C. L. Chan (1984), Comments on "A numerical study of the interaction between two tropical cyclones," *Mon. Weather Rev.*, *112*, 1643–1645.

Derber, J. C., and W.-S. Wu (1998), The use of TOVS cloud-cleared radiances in the NCEP SSI analysis system, *Mon. Weather Rev.*, *126*, 2287–2299.

Desroziers, G., and S. Ivanov (2001), Diagnosis and adaptive tuning of observation-error parameters in a variational assimilation, *Quart. J. R. Meteorol. Soc.*, *127*, 1433–1452.

Dong, K., and C. J. Neumann (1983), On the relative motion of binary tropical cyclones, *Mon. Weather Rev.*, *111*, 945–953.

Fiorino, M. (2009), Record-setting performance of the ECMWF IFS in medium-range tropical cyclone track prediction, *ECMWF Newsl.* 118, pp. 20–27, Eur. Cent. for Medium-Range Weather Forecasts, Reading, U. K.

Fujiwhara, S. (1921), The mutual tendency towards symmetry of motion and its application as a principle in meteorology, *Quart. J. R. Meteorol. Soc.*, *47*, 287–293.

Fujiwhara, S. (1923), On the growth and decay of vortical systems, *Quart. J. R. Meteorol. Soc.*, *49*, 75–104.

Hamill, T. M. (1999), Hypothesis tests for evaluating numerical precipitation forecasts, *Weather Forecasting*, *14*, 155–167.

Hamill, T. M., J. S. Whitaker, M. Fiorino, and S. G. Benjamin (2011), Global ensemble predictions of 2009's tropical cyclones initialized with an ensemble Kalman filter, *Mon. Weather Rev.*, *139*, 668–688.

Han, Y., P. van Delst, Q. Liu, F. Weng, B. Yan, R. Treadon, and J. Derber (2006), JCSDA Community Radiative Transfer Model (CRTM), Version 1, *NOAA Tech. Rep. NESDIS 122*, 33 pp., National Oceanic and Atmospheric Administration (NOAA), Washington, D. C.

Hong, S.-Y., and J.-O. J. Lim (2006), The WRF single-moment 6-class microphysics scheme (WSM6), *J. Korean Meteorol. Soc.*, *42*, 129–151.

Hong, S.-Y., Y. Noh, and J. Dudhia (2006), A new vertical diffusion package with an explicit treatment of entrainment processes, *Mon. Weather Rev.*, *134*, 2318–2341.

Iacono, M. J., J. S. Delamere, E. J. Mlawer, M. W. Shephard, S. A. Clough, and W. D. Collins (2008), Radiative forcing by long-lived greenhouse gases: Calculations with the AER radiative transfer models, *J. Geophys. Res.*, *113*, D13103, doi:10.1029/2008JD009944.

Jang, W., and H.-Y. Chun (2015a), Characteristics of binary tropical cyclones observed in the western North Pacific for 62 years (1951–2012), *Mon. Weather Rev.*, *143*, 1749–1761.

Jang, W., and H.-Y. Chun (2015b), Effects of thermodynamic profiles on the interaction of binary tropical cyclones, *J. Geophys. Res.*, *120*, 9173–9192, doi:10.1002/2015JD023409.

Jarrell, J., S. Brand, and D. S. Nicklin (1978), An analysis of western North Pacific tropical cyclone forecast errors, *Mon. Weather Rev.*, *106*, 925–937.

Joo, S., J. Eyre, and R. Marriott (2013), The impact of MetOp and other satellite data within the Met Office global NWP system using an adjoint-based sensitivity method, *Mon. Weather Rev.*, *141*, 3331–3342.

Kain, J. S. (2004), The Kain-Fritsch convective parameterization: An update, *J. Appl. Meteorol.*, *43*, 170–181.

Kazumori, M., A. J. Geer, and S. J. English (2016), Effects of all-sky assimilation of GCOM-W/AMSR2 radiances in the ECMWF numerical weather prediction system, *Quart. J. R. Meteorol. Soc.*, *142*, 721–737.

Khain, A., I. Ginis, A. Falkovich, and M. Frumin (2000), Interaction of binary tropical cyclones in a coupled tropical cyclone-ocean model, *J. Geophys. Res.*, *105*, 22,337–22,354.

Kuo, H.-C., G. T.-J. Chen, and C.-H. Lin (2000), Merger of tropical cyclones Zeb and Alex, *Mon. Weather Rev.*, *128*, 2967–2975.

Lander, M. A., and G. J. Holland (1993), On the interaction of tropical-cyclone-scale vortices. I: Observation, *Quart. J. R. Meteorol. Soc.*, *119*, 1347–1361.

Liu, H., J. Anderson, Y.-H. Kuo, and K. Raeder (2007), Importance of forecast error multivariate correlations in idealized assimilation of GPS radio occultation data with the ensemble adjustment filter, *Mon. Weather Rev.*, *135*, 17–185.

Liu, Q., and F. Weng (2006), Advanced doubling-adding method for radiative transfer in planetary atmosphere, *J. Atmos. Sci.*, *63*, 3459–3465.

Liu, Z., and F. Rabier (2002), The interaction between model resolution, observation resolution, and observation density in data assimilation: A one-dimensional study, *Quart. J. R. Meteorol. Soc.*, *128*, 1367–1386.
Liu, Z., C. S. Schwartz, C. Snyder, and S.-Y. Ha (2012), Impact of assimilating AMSU-A radiances on forecasts of 2008 Atlantic tropical cyclones initialized with a limited-area ensemble Kalman filter, *Mon. Weather Rev.*, *140*, 4017–4034.
Lorenc, A. C., N. E. Bowler, A. M. Clayton, S. T. Pring, and D. Fairbairn (2015), Comparison of hybrid-4DEnVar and hybrid-4DVar data assimilation methods for global NWP, *Mon. Weather Rev.*, *143*, 212–229.
McNally, A. P., and P. D. Watts (2003), A cloud detection algorithm for high-spectral-resolution infrared sounders, *Quart. J. R. Meteorol. Soc.*, *129*, 3411–3423.
McNally, A. P., J. C. Derber, W. Wu, and B. B. Katz (2000), The use of TOVS level-1b radiances in the NCEP SSI analysis system, *Quart. J. R. Meteorol. Soc.*, *126*, 689–724.
McNally, T. (2007), The use of satellite data in polar regions, in *Proceedings of the ECMWF Seminar on Polar Meteorology*, pp. 103–114, Eur. Cent. for Medium-Range Weather Forecasts, Reading, U. K.
Newman, K. M., C. S. Schwartz, Z. Liu, H. Shao, and X.-Y. Huang (2015), Evaluating forecast impact of assimilating Microwave Humidity Sounder (MHS) radiances with a regional ensemble Kalman filter data assimilation system, *Weather Forecasting*, *30*, 964–983.
Parrish, D. F., and J. C. Derber (1992), The National Meteorological Center's spectral statistical interpolation analysis system, *Mon. Weather Rev.*, *120*, 1747–1763.
Prieto, R., B. D. McNoldy, S. R. Fulton, and W. H. Schubert (2003), A classification of binary tropical cyclone-like vortex interactions, *Mon. Weather Rev.*, *131*, 2656–2666.
Rappaport, E. N., et al. (2009), Advances and challenges at the National Hurricane Center, *Weather Forecasting*, *24*, 395–419.
Ritchie, E. A., and G. J. Holland (1993), On the interaction of tropical-cyclone-scale vortices. II: Discrete vortex patches, *Quart. J. R. Meteorol. Soc.*, *119*, 1363–1379.
Saba, V. S., et al. (2016), Enhanced warming of the Northwest Atlantic Ocean under climate change, *J. Geophys. Res. Oceans*, *121*, 118–132, doi:10.1002/2015JC011346.
Schwartz, C. S., Z. Liu, Y. Chen, and X.-Y. Huang (2012), Impact of assimilating microwave radiances with a limited-area ensemble data assimilation system on forecasts of Typhoon Morakot, *Weather Forecasting*, *27*, 424–437.
Singh, R., C. M. Kishtawal, P. K. Pal, and P. C. Joshi (2011), Assimilation of the multisatellite data into the WRF model for track and intensity simulation of the Indian Ocean tropical cyclones, *Meteorol. Atmos. Phys.*, *111*, 103–119.
Singh, R., C. M. Kishtawal, P. K. Pal, and P. C. Joshi (2012), Improved tropical cyclone forecasts over north Indian Ocean with direct assimilation of AMSU-A radiances, *Meteorol. Atmos. Phys.*, *115*, 15–34.
Skamarock, W. C., J. B. Klemp, J. Dudhia, D. O. Gill, D. M. Barker, M. G. Duda, X.-Y. Huang, W. Wang, and J. G. Powers (2008), A description of the advanced research WRF version 3, *NCAR Tech. Note NCAR/TN-475+STR*, 113 pp., National Center for Atmospheric Research (NCAR), Boulder, Colo.
Wang, Y., and G. J. Holland (1995), On the interaction of tropical-cyclone-scale vortices. IV: Baroclinic vortices, *Quart. J. R. Meteorol. Soc.*, *121*, 95–126.
Wijffels, S., D. Roemmich, D. Monselesan, J. Church, and J. Gilson (2016), Ocean temperatures chronicle the ongoing warming of Earth, *Nat. Clim. Change*, *6*, 116–118.
Wu, C.-C., T.-S. Huang, W.-P. Huang, and K.-H. Chou (2003), A new look at the binary interaction: Potential vorticity diagnosis of the unusual southward movement of Tropical Storm Bopha (2000) and its interaction with Supertyphoon Saomai (2000), *Mon. Weather Rev.*, *131*, 1289–1300.
Wu, X., J.-F. Fei, X.-G. Huang, X.-P. Cheng, and J.-Q. Ren (2011), Statistical classification and characteristics analysis of binary tropical cyclones over the western North Pacific Ocean, *J. Trop. Meteorol.*, *17*, 335–344.
Wu, X., J.-F. Fei, X.-G. Huang, X. Zhang, X.-P. Cheng, and J.-Q. Ren (2012), A numerical study of the interaction between two simultaneous storms: Goni and Morakot in September 2009, *Adv. Atmos. Sci.*, *29*, 561–574.
Xu, D., Z. Liu, X.-Y. Huang, J. Min, and H. Wang (2013), Impact of assimilating IASI radiance observations on forecasts of two tropical cyclones, *Meteorol. Atmos. Phys.*, *122*, 1–18.
Xu, D., X.-Y. Huang, H. Wang, A. P. Mizzi, and J. Min (2015), Impact of assimilating radiances with the WRFDA ETKF/3DVAR hybrid system on prediction of two typhoons in 2012, *J. Meteorol. Res.*, *29*, 28–40.
Xu, D., J. Min, F. Shen, J. Ban, and P. Chen (2016), Assimilation of MWHS radiance data from the FY-3B satellite with the WRF Hybrid-3DVAR system for the forecasting of binary typhoons, *J. Adv. Model. Earth Syst.*, *8*, 1014–1028, doi:10.1002/2016MS000674.
Zapotocny, T. H., J. A. Jung, J. F. Le Marshall, and R. E. Treadon (2008), A two-season impact study of four satellite data types and rawinsonde data in the NCEP Global Data Assimilation System, *Weather Forecasting*, *23*, 80–100.
Zhang, S., T. Li, X. Ge, M. Peng, and N. Pan (2012), A 3DVAR-based dynamical initialization scheme for tropical cyclone predictions, *Weather Forecasting*, *27*, 473–483.
Zhu, Y., and R. Gelaro (2008), Observation sensitivity calculations using the adjoint of Gridpoint Statistical Interpolation (GSI) analysis system, *Mon. Weather Rev.*, *136*, 335–351.
Zhu, Y., E. Liu, R. Mahahan, C. Thomas, D. Groff, P. V. Delst, A. Collard, D. Kleist, R. Treadon, and J. C. Derber (2016), All-sky microwave radiance assimilation in the NCEP's GSI analysis system, *Mon. Weather Rev.*, *144*, 4709–4735, doi:10.1175/MWR-D-15-0445.1.
Zou, X., F. Weng, B. Zhang, L. Lin, Z. Qin, and V. Tallapragada (2013a), Impacts of assimilation of ATMS data in HWRF on track and intensity forecasts of 2012 four landfall hurricanes, *J. Geophys. Res.*, *118*, 11,558–11,576, doi:10.1002/2013JD020405.
Zou, X., Z. Qin, and F. Weng (2013b), Improved quantitative precipitation forecasts by MHS radiance data assimilation with a newly added cloud detection algorithm, *Mon. Weather Rev.*, *141*, 3203–3221.